NASA Technical Memorandum 104566, Vol. 29

SeaWiFS Technical Report Series

Stanford B. Hooker, Editor
Goddard Space Flight Center
Greenbelt, Maryland

Elaine R. Firestone, Technical Editor
General Sciences Corporation
Laurel, Maryland

Volume 29, The SeaWiFS CZCS-Type Pigment Algorithm

James Aiken and Gerald F. Moore
Plymouth Marine Laboratory
Plymouth, United Kingdom

Charles C. Trees
San Diego State University
San Diego, California

Stanford B. Hooker
NASA Goddard Space Flight Center
Greenbelt, Maryland

Dennis K. Clark
NOAA/National Environmental Satellite
Data Information Service
Camp Springs, Maryland

J. Aiken, G.F. Moore, C.C. Trees, S.B. Hooker, and D.K. Clark

ABSTRACT

The Sea-viewing Wide Field-of-view Sensor (SeaWiFS) mission will provide operational ocean color that will be superior to the previous Coastal Zone Color Sensor (CZCS) proof-of-concept mission. An algorithm is needed that exploits the full functionality of SeaWiFS whilst remaining compatible in concept with algorithms used for the CZCS. This document describes the theoretical rationale of radiance band-ratio methods for determining chlorophyll a and other important biogeochemical parameters, and their implementation for the SeaWIFS mission. Pigment interrelationships are examined to explain the success of the CZCS algorithms. In the context where chlorophyll a absorbs only weakly at 520 nm, the success of the 520 nm to 550 nm CZCS band ratio needs to be explained. This is explained by showing that in pigment data from a range of oceanic provinces chlorophyll a (absorbing at less than 490 nm), carotenoids (absorbing at greater than 460 nm), and total pigment are highly correlated. Correlations within pigment groups particularly photoprotectant and photosynthetic carotenoids are less robust. The sources of variability in optical data are examined using the NIMBUS Experiment Team (NET) bio-optical data set and bio-optical model. In both the model and NET data, the majority of the variance in the optical data is attributed to variability in pigment (chlorophyll a), and total particulates, with less than 5% of the variability resulting from pigment assemblage. The relationships between band ratios and chlorophyll is examined analytically, and a new formulation based on a dual hyperbolic model is suggested which gives a better calibration curve than the conventional log-log linear regression fit. The new calibration curve shows the 490:555 ratio is the best single-band ratio and is the recommended CZCS-type pigment algorithm. Using both the model and NET data, a number of multiband algorithms are developed; the best of which is an algorithm based on the 443:555 and 490:555 ratios. From model data, the form of potential algorithms for other products, such as total particulates and dissolved organic matter (DOM), are suggested.

1. INTRODUCTION

As a second-generation ocean color instrument, the Sea-viewing Wide Field-of-view Sensor (SeaWiFS) offers a variety of design improvements over its predecessor the Coastal Zone Color Scanner (CZCS). The design of the SeaWiFS instrument was driven by science requirements as defined by the SeaWiFS Prelaunch Science Working Group (SP-SWG). The SPSWG was an ad hoc committee selected by the National Aeronautics and Space Administration (NASA) Headquarters for the purpose of providing NASA with guidance in the formulation of mission objectives, specifications, and goals. The SPSWG has specifically expressed a requirement for continuity between CZCS and SeaWiFS products.

Consequently, the SeaWiFS Project Office (SPO) plans to produce three groups of level-2 derived products: SeaWiFS *baseline*, *CZCS-type*, and *potential* SeaWiFS products. A differentiation is made between CZCS-type pigment and SeaWiFS baseline *chlorophyll-like* pigment concentrations. The SeaWiFS semianalytical algorithm for chlorophyll a will be developed using analytical and semi-analytical models. Chlorophyll a is the parameter that has been chosen as it is regarded universally as the most appropriate measure of viable phytoplankton biomass (i.e., phytoplankton which are growing actively and capable of growth).

The CZCS-type pigment product is supposed to provide some form of continuity with the *total pigment* prod-uct derived from CZCS imagery, termed the *CZCS Pigment Algorithm* product. There is no predetermined consensus for the rationale or definition of this product (chlorophyll a, photosynthetic pigments, or total pigments). A choice must be made at the outset, so a methodological approach can be determined and described. The proposed approach should be essentially empirical, and use band ratios in common with the original CZCS algorithms. There is a strong desire in the community, for example, the Bio-Optical Algorithm Working Group (BOAWG), that there should be a SeaWiFS product compatible with the CZCS imagery, so retrospective processing can be applied and comparability between CZCS and SeaWiFS data can be achieved.

To derive global bio-mass and productivity trends on decadal time scales, it is possible the standard NASA CZCS two-band algorithm, used for the global processing, could be used unaltered. It may be that an algorithm using all three bands at 443, 520, and 550 nm, however, would give a more statistically robust relationship; these bands are close to the SeaWiFS 443, 510, and 555 nm bands and continuity would seem likely in this case.

This hypothesis is flawed logically in a number of respects, primarily because of the differences between the CZCS and SeaWiFS instruments (Hooker et al. 1993). SeaWiFS will have precision radiometry (10 bit resolution), precision calibration (prelaunch and onboard), stability of calibration monitoring, and established vicarious calibration schemes—CZCS had nothing comparable. SeaWiFS

will have two infrared (IR) bands (765 and 865 nm) which will allow for precision atmospheric correction, whereas CZCS atmospheric correction was limited and often failed (many of the assumptions necessary for CZCS atmospheric correction were invalid, e.g., often the 670 nm band was not truly a zero water-leaving radiance band); SeaWiFS will have at least five precision atmospherically corrected bands (whereas CZCS had three) offering a greater potential for multiband algorithms of widespread applicability. In fact, the only strictly comparable feature between the CZCS and SeaWiFS instruments is the common blue band at 443 nm.

The radical difference between the atmospheric correction schemes may mean that comparability will be limited. It is likely the best SeaWiFS band-ratio algorithms will use three, four, or five visible bands not compatible with CZCS: three bands using 412, 443, and 555 nm or 443, 490, and 555 nm; four bands using 412, 443, 490 (or 510), and 555 nm; or five bands using 412, 443, 490, 510, and 555 nm. The BOAWG team has agreed that besides the CZCS-type pigment algorithm, there should be continued research to identify the best possible SeaWiFS pigment algorithm.

The objective of this study is to provide a band-ratio algorithm that has the best possible continuity with CZCS measurements. The focus of attention, however, is on the derivation of the best possible band-ratio algorithm for the retrieval of phytoplankton pigments from SeaWiFS observations. The desire is to achieve these goals based on a sound theoretical basis and rationale.

2. PIGMENTS REVISITED

The product from the CZCS pigment algorithm was chlorophyll a plus phaeopigment concentration, $C_a + C_P$ (as determined by the fluorometric method), which were considered the main absorbing agents of biogenic origin by the NIMBUS Experiment Team (NET). The reasons for the choice of the $C_a + C_P$ parameter was partly historical and partly methodological. Prior to 1980, the principle methods for the determination of chlorophyll a were the tri-chrometric spectrometric method (Strickland and Parsons 1972) and the fluorescence method (Yentsch and Menzel 1963). Both methods could be imprecise (e.g., at low concentrations) and frequently under- and over-estimated both C_a and C_P due to the presence of other interfering pigments, notably chlorophyll b and chlorophyll c.

It is now accepted by most biological oceanographers that phaeopigments rarely exceed 3–8% of the total pigment concentration in the surface layer of the ocean, with the exception of a few well understood circumstances, for example, when zooplankton grazing is high and localized. Furthermore, there are a number of other photosynthetic and photoprotectant pigments which co-exist, co-vary, and absorb at the same wavelengths as chlorophyll a, and which occur in significant concentrations. Individually, they may account for approximately 5–50% of the total pigment concentration and, in combination with chlorophyll a, may contribute to over 95% of the total pigment biomass. Most of these have an important influence on water color at the wavelengths of the SeaWiFS bands. An accurate assessment would involve the sum of the optically weighted contribution of the main pigments present for different natural phytoplankton assemblages in different geographical sites and seasons.

A comment on pigment measurement techniques is appropriate here. Much of the insight into the composition and significance of differing phytoplankton pigments has come as a result of the development of analyses using the high performance liquid chromatography (HPLC) technique (Mantoura and Llewellyn 1983 and Trees et al. 1985), which is the recommended methodology in the *Ocean Optics Protocols for SeaWiFS Validation* (Mueller and Austin 1995).

Along with the insight on pigments for some has come confusion for others, with earlier reports that concentrations of pigments determined by HPLC and fluorescence (Trees et al. 1985) differed markedly—much lower pigment concentrations were obtained using the HPLC technique. A thorough investigation by Trees et. al (1995) has shown that when each method is applied rigorously, each yields about one-to-one ($\pm 10\%$) relationships for chlorophyll a in most bio-optical provinces. Errors can arise, however, if the protocols for sampling, filtration, extraction, and calibration are not adhered to strictly; exceptions occur if either chlorophyll b or chlorophyll c are atypically high (greater than about 5% of the total).

Recently, there have been several studies investigating the contribution of the major phytoplankton pigments to light absorption in the oceans, including the independent analyses by Bidigare et al. (1990) as well as Hoepffner and Sathyendranath (1993). Although the latter study was restricted to samples from the Georges Bank area, both studies showed the major pigments that need to be included to account for 95% of the light absorbed are relatively few in number:

1) Chlorophylls a, b, and c;

2) The photosynthetic carotenoids (PSC); and

3) The photoprotectant carotenoids (PPC).

In the yellow-orange part of the spectrum (at around 550 nm), the phycobilin, phycoerythrin, and phycocyanin pigments are moderately important light absorbers. These pigments occur mostly in cyanobacteria, which are generally unimportant in the surface layers of the ocean relevant to this study; the only known instances of significance correspond to blooms of cyanobacteria occurring in upwelling regions. Other, taxa-specific, tag-pigments are also insignificant to the total light absorption in the ocean—individually or collectively they account for less than 5% of the absorption. Both Bidigare et al. (1990) and Hoepffner and Sathyendranath (1993) give tables of the specific absorption coefficients of these major pigment groups. Although there is general agreement between these

Table 1. Total pigment concentration (C_{TP}) to chlorophyll a (C_a) relationships.

C_{TP}	R^2	N	Comments
$0.021 + 2.17C_a$	95.5	670	All data.
$-0.040 + 2.30C_a$	95.9	630	$C_a \leq 3\,\mathrm{mg\,m^{-3}}$
$0.031 + 2.16C_a$	93.2	416	$z \leq 10\,\mathrm{m}$

Table 2. Global total pigment regressions†.

Region	C_a	R^2	C_b	R^2	C_c	R^2	C_{abc}	R^2	C_{PP}	R^2	C_{PS}	R^2
Antarctic	0.544	97.3	0.006	35.7	0.154	79.6	0.295	98.8	0.043	45.4	0.252	96.2
NEAT 89–90	0.422	99.6	0.016	76.6	0.134	99.5	0.427	99.3	0.049	83.5	0.377	99.5
NEAT 91‡	0.519	98.6	0.024	27.1	0.020	86.3	0.436	97.4	0.122	80.5	0.313	92.5
GIN Seas	0.367	96.6	0.085	74.6	0.103	88.8	0.443	95.0	0.096	68.8	0.346	94.9
Georges Bank	0.525	98.8	0.066	84.4	0.051	98.2	0.358	98.5	0.104	96.9	0.253	97.7
Bermuda (BATS)	0.499	99.6	0.026	52.6	0.036	89.7	0.437	99.4	0.231	98.7	0.207	98.8
EqPac	0.446	99.7	0.074	93.6	0.042	91.4	0.436	99.2	0.249	94.5	0.186	97.1
Global	0.475		0.042		0.077		0.407		0.128		0.276	

† Regression assumes no intercept.   ‡ NEAT 1991 is coccolithophore bloom data.

two different studies, there is some divergence concerning the coefficients in the blue spectral region.

Figure 1a, from Bidigare et al. (1990), shows the weight-specific absorption coefficient for the major pigment groups, and Fig. 1b shows the equivalent figure from Hoepffner and Sathyendranath (1993). Figure 2 shows the actual pigment absorption for the major pigments and the summed total for measurements from a cruise to the Northeast Atlantic (NEAT) in June 1991 (Holligan et al. 1993). For the latter, the phytoplankton assemblage was dominated by cocco-lithophores and small flagellates, yet these data are similar to the earlier studies with the total pigment absorption dominated by chlorophyll a, PSC, and PPC—chlorophyll b and chlorophyll c have less than 5% significance.

Bidigare et al. (1990) concluded accessory pigments do not always co-vary with chlorophyll a over depth and time. In this study, the relationships of accessory pigments to chlorophyll a for the surface layers only, sensed by satellite color imagers, are examined using data from a wide variety of sources (published and unpublished). An examination of the relationship between chlorophyll a and total pigments (sum of chlorophylls a, b, c, PSC, and PPC) shows a robust relationship (97% of the variance explained). Nearly 5,600 pigment determinations from many bio-optical provinces were used in the analysis (see Fig. 3). Province by province and cruise by cruise, the ratio of total pigment to chlorophyll a varied from 1.876–2.876 with a mean of 2.164.

The conclusion from this analysis could be that it matters little whether the algorithm product is chlorophyll a or total pigments, since the relationship between these two measures of marine phytoplankton biomass, on a global level, are so tightly coupled. Two issues make this hypothesis invalid:

1. The optical influence of the different pigment groups (e.g., the chlorophylls and carotenoids) are quite dif-

ferent in the five SeaWiFS blue and green bands (412, 443, 490, 510, and 555 nm).

2. The relative composition of carotenoids (e.g., PSC) in different biogeographical (bio-optical) provinces is not constant and varies significantly from cruise to cruise and province to province.

This is demonstrated here by a thorough analysis of all pigment interrelationships for seven widely differing bio-geochemical (bio-optical) provinces:

- Greenland, Iceland, and Norwegian (GIN) Seas 1986–87 (Trees),
- Georges Bank (Hoepffner and Sathyendranath 1992),
- NEAT 1989–90 (United Kingdom) Biogeochemical Ocean Flux Study (BOFS),
- NEAT 1991 BOFS (Trees),
- Equatorial Pacific (EqPac) 1992 (Spring and Fall),
- Antarctica 1992 BOFS (Sterna), and
- Bermuda Atlantic Time-Series Station (BATS).

Note that the total pigment to chlorophyll a relationships for all combined data are highly correlated as shown in Table 1, with the major pigment relationships shown in Fig. 4. Examining the data province by province, it is evident there are widely varying ratios of the concentrations of chlorophylls a, b, c, PPC, and PSC $(C_a, C_b, C_c, C_{PP}$, and C_{PS}, respectively) to total pigment concentration (C_{TP}) as shown in Table 2 and Fig. 5a–g.

This analysis shows that for chlorophyll a, chlorophyll c, total carotenoids, and PSC, the intraprovince covariance is extremely tight for all provinces (R^2 is 96–99% for chlorophyll a to C_{TP}), although the coefficients of variance differ: notably, the fraction of chlorophyll a is lowest in the
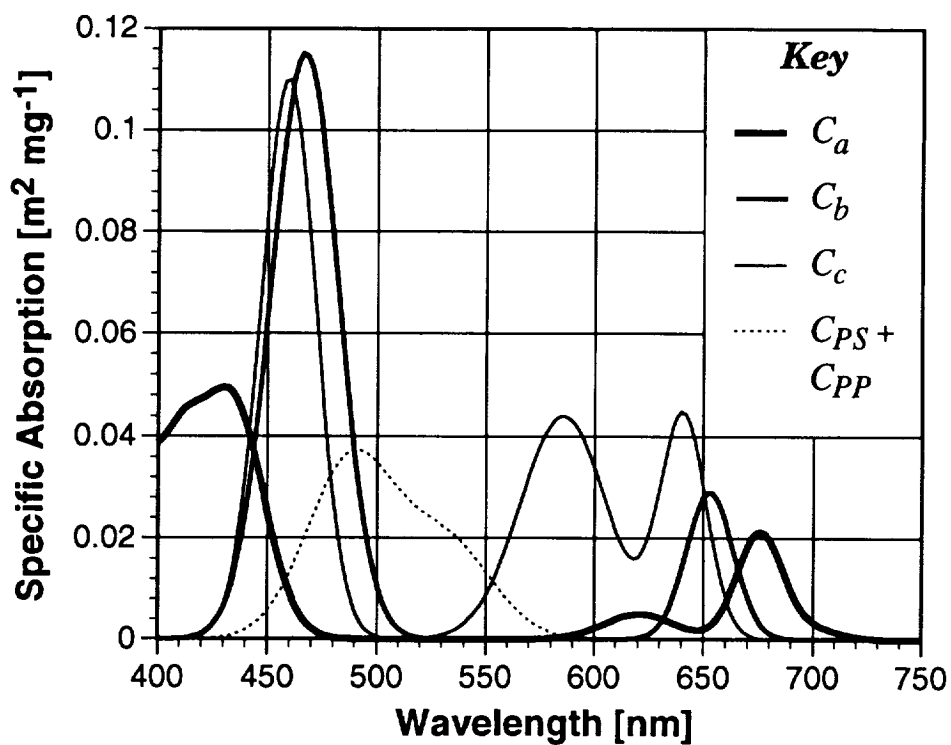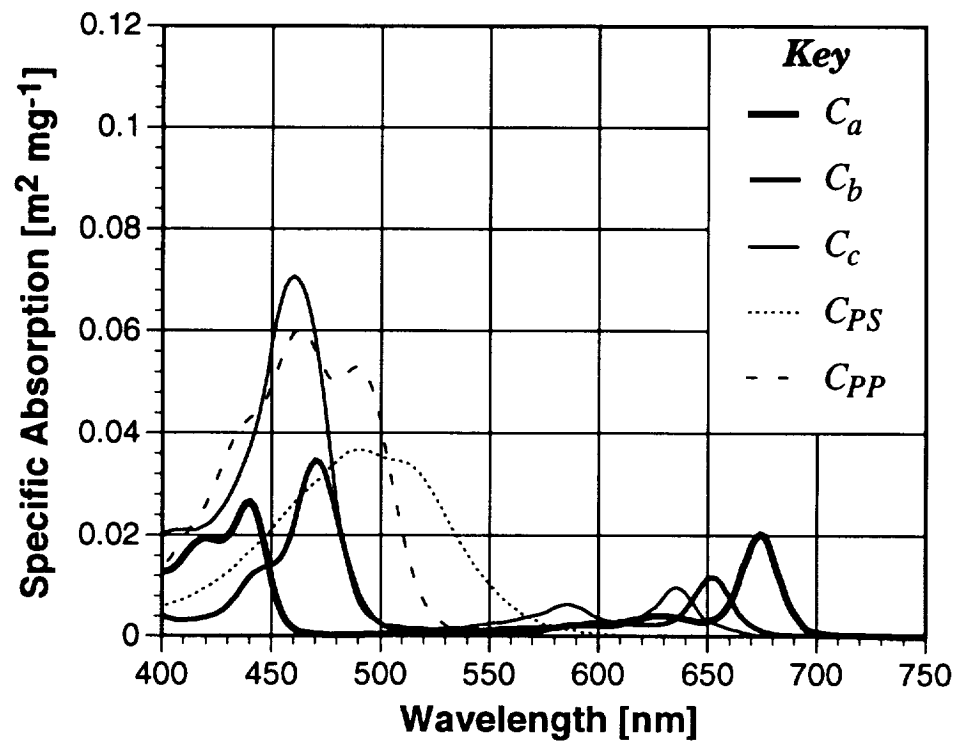
Fig. 1. Pigment-specific absorption versus wavelength from a) Bidigare et al. (1990) and b) Hoepffner and Sathyendranath (1993), top and bottom plots, respectively.
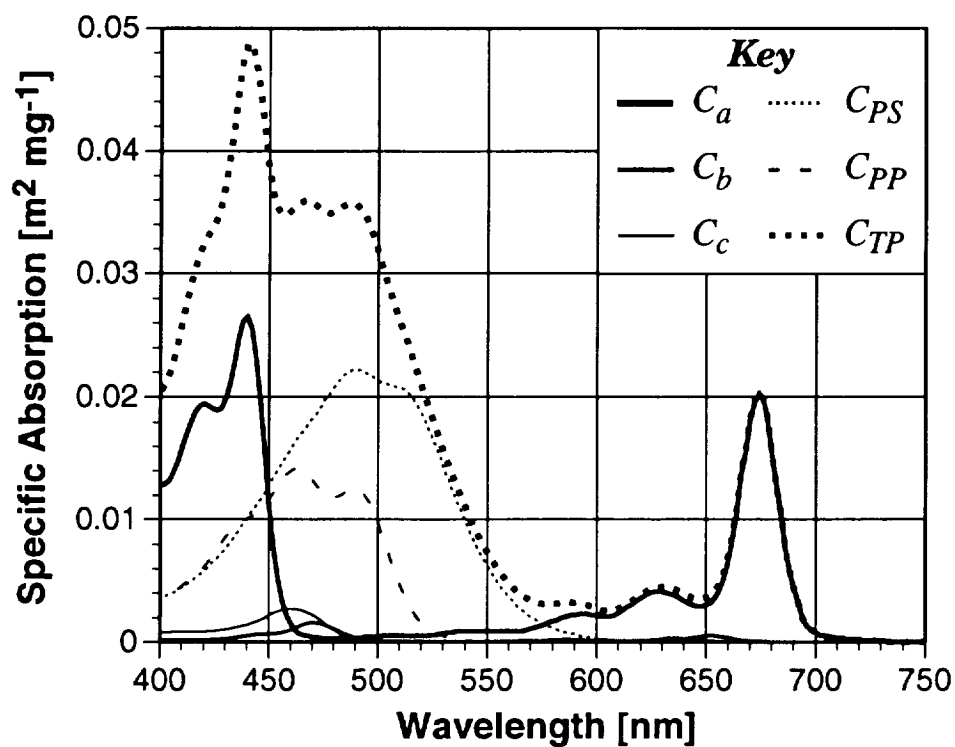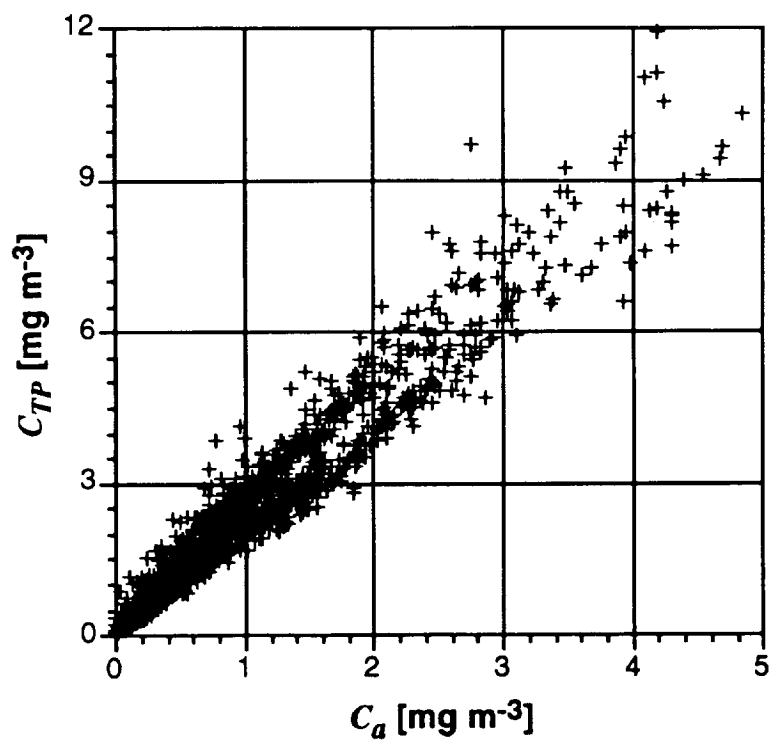
Fig. 2. Simulated pigment absorption.

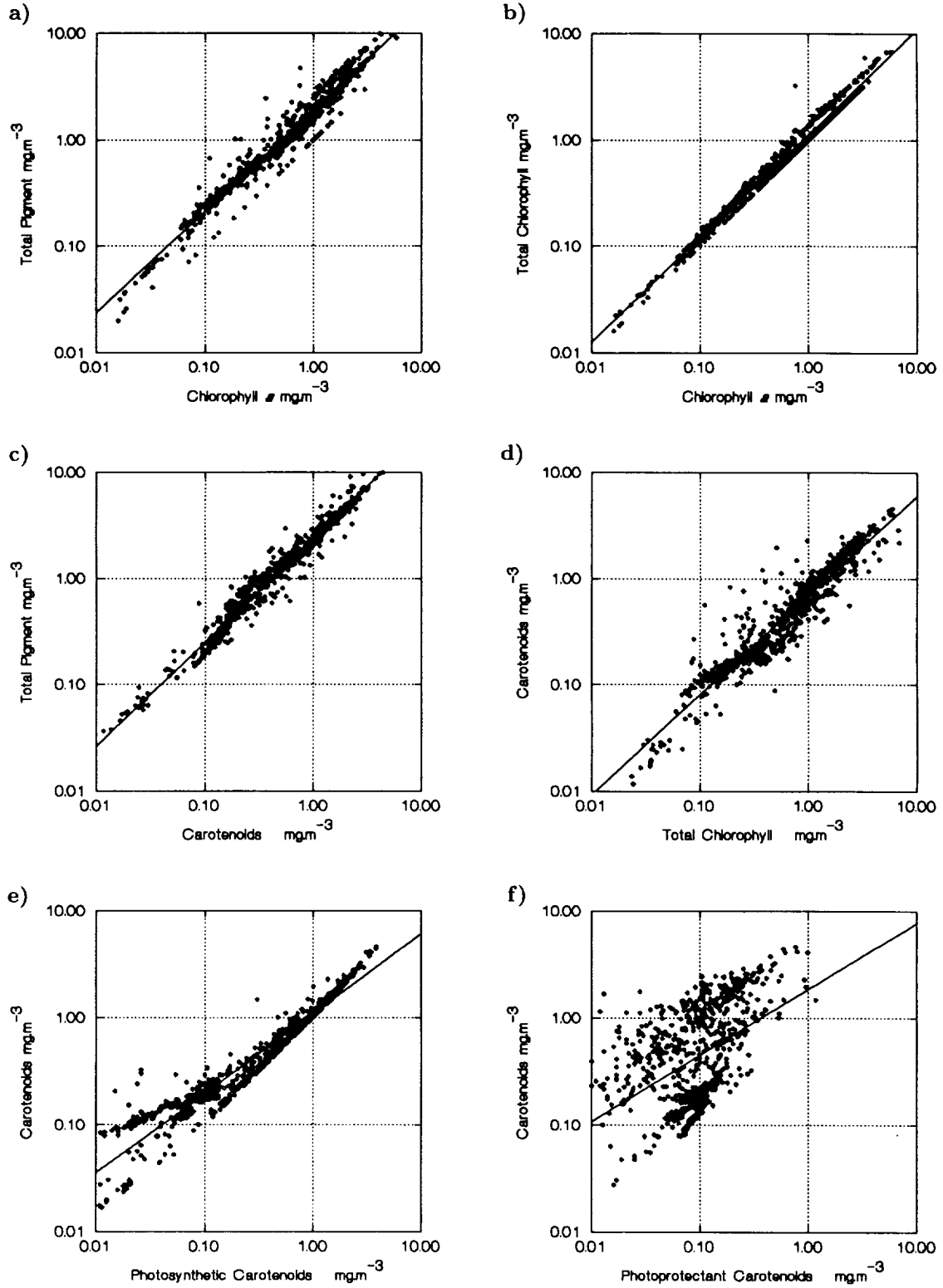**Fig. 3.** Chlorophyll a versus total pigments.

Fig. 4. Pigment regressions: **a)** $C_{TP} = 0.13 + 1.96C_a$ (R^2=93.2%), **b)** $C_{abc} = 0.02 + 1.20C_a$ (R^2=97.6%), **c)** $C_{TP} = 0.13 + 2.27[C_{PP} + C_{PS}]$ (R^2=93.7%), **d)** $C_{PP} + C_{PS} = 0.12 + 0.76C_{abc}$ (R^2=77.5%), **e)** $C_{PP} + C_{PS} = 0.03 + 1.15C_{PS}$ (R^2=97.5%), and **f)** $C_{PP} + C_{PS} = 0.41 + 3.67C_{PP}$ (R^2=56.2%).
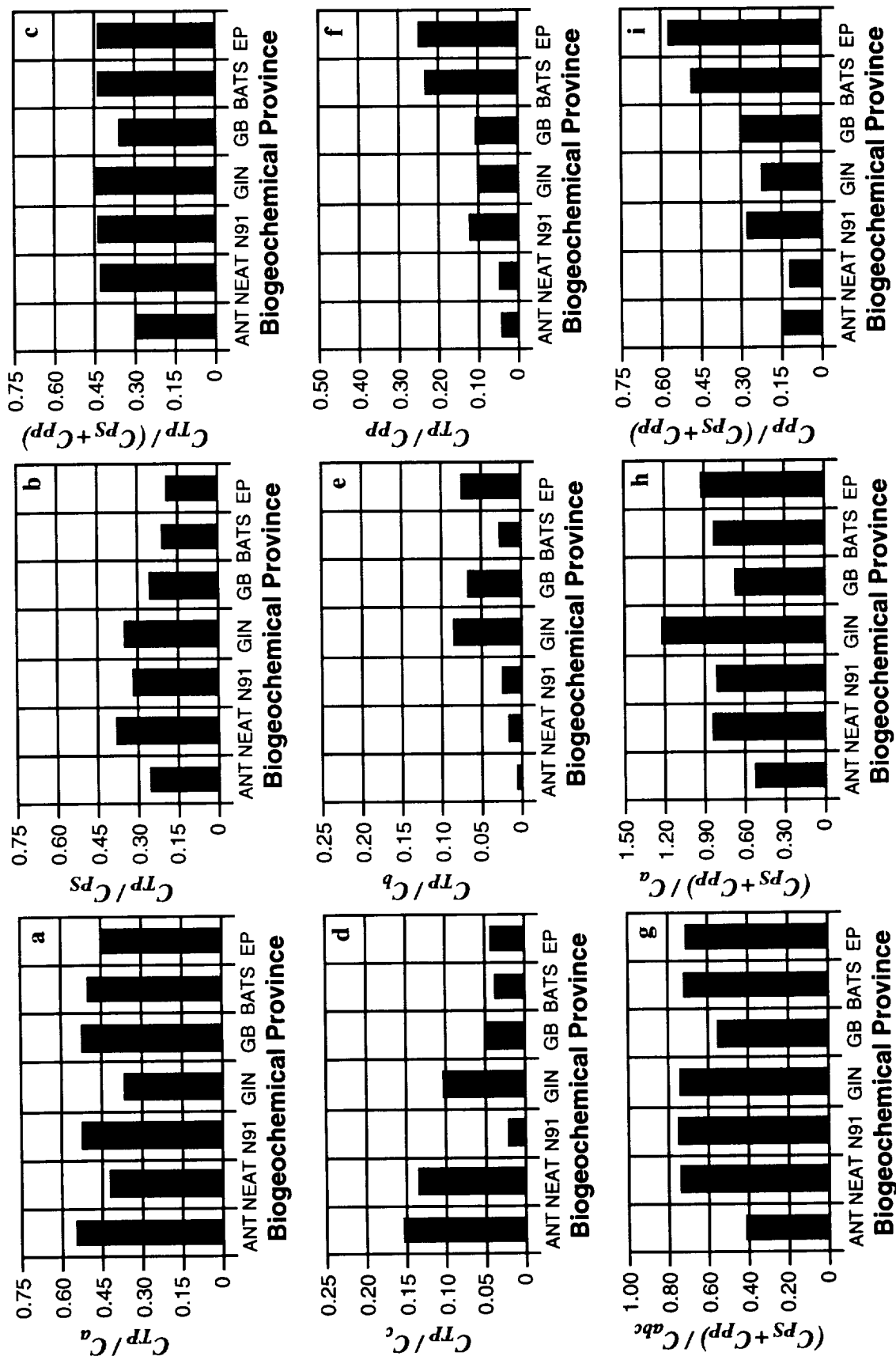
Fig. 5. Global total pigment ratios for a variety of biogeochemical provinces: **a)** C_{TP}/C_a, **b)** C_{TP}/C_{PS}, **c)** $C_{TP}/(C_{PS}+C_{PP})$, **d)** C_{TP}/C_c, **e)** C_{TP}/C_b, **f)** C_{TP}/C_{PP}, **g)** $(C_{PS}+C_{PP})/C_{abc}$, **h)** $(C_{PS}+C_{PP})/C_a$, and **i)** $C_{PP}/(C_{PS}+C_{PP})$. The provinces are encoded as follows: Antarctica (ANT), NEAT (NEAT 89–90), N91 (NEAT 91), GIN Seas (GIN), Grand Banks (GB), BATS, and EqPac (EP).

GIN Seas (0.367), and highest in Antarctica (0.514). The low fraction in the GIN Seas is partly compensated by the high fraction of chlorophyll b (0.085) and chlorophyll c (0.103). In contrast, the fraction of carotenoids, mostly PSC, is lowest in Antarctica (0.295) and relatively constant elsewhere; relative to chlorophyll a, there are substantially more carotenoids in the GIN Seas than anywhere else and only here are they the major pigment group and exceed the fraction for chlorophyll a.

The global mean fraction of chlorophyll a is close to 0.5 (depressed only by the GIN Seas data), whereas, the global mean fraction of total carotenoids is about 0.4. The global mean fractions of chlorophylls b and c are 0.042 and 0.077, respectively, and are most significant in the GIN Seas. Chlorophyll b is practically insignificant in the Antarctica, NEAT, and the BATS data. The global mean fraction of PPC is 0.128, over 20% of the total pigment composition in BATS and EqPac data (both of which are high light) and relatively low in the Antarctica (0.043) and NEAT 89-90 data, both of which are low light environments.

The extremes of the interpigment variance, from province to province, is highlighted in Table 3 and Figs. 5g-i, which shows the ratio of total carotenoids $(C_{PP} + C_{PS})$ to chlorophyll a (C_a), and to total chlorophyll (C_{abc}). The latter being the sum of chlorophylls a, b, and c. The lowest ratio (0.522) is found in Antarctica and the highest ratio (1.129) is found in the GIN Seas. These extremes are reduced somewhat if the carotenoid to total chlorophyll ratio is considered (0.416 for Antarctica and 0.738 for the GIN Seas).

Table 3. Global interpigment ratios†.

Region	$\frac{C_{PP}+C_{PS}}{C_a}$	R^2	$\frac{C_{PP}+C_{PS}}{C_{abc}}$	R^2
Antarctic	0.522	94.3	0.416	97.9
NEAT 89–90	0.835	94.8	0.735	97.2
NEAT 91	0.814	92.9	0.745	91.9
GIN Seas	1.129	86.3	0.738	84.5
Georges Bank	0.665	95.0	0.549	96.3
BATS	0.824	98.8	0.715	98.3
EqPac	0.911	98.2	0.711	97.2
Global	0.814		0.658	

† Regression assumes no intercept.

Using the radiances $L_{WN}(443)$ and $L_{WN}(550)$, these differences in the relative pigment concentrations would lead to significant differences in the coefficients of a standard two-band algorithm for each of these different biogeochemical (bio-optical) provinces, because of the different contributions to the optical absorption from each pigment at 443 and 550 nm. It is likely that multiband algorithms (3, 4, and 5 wavelengths) designed to account for the influences of different pigments on the absorption at each waveband, may produce algorithms that would have more widespread application.

3. BAND-RATIO ALGORITHMS

The approach adopted here, in line with the tried and tested methods used for CZCS, is essentially empirical, although, as is the case with the mainstream semianalytical SeaWiFS algorithm for chlorophyll a, the methods are validated by recourse to standard bio-optical, hydrological models. By this means, semi-empirical algorithms are developed, whereby analytical methods are used to propose the form of the algorithm, while empirical methods are used to determine the numerical coefficients.

The two-band (blue to green ratio) algorithms used for CZCS, developed by empirical methods (Clark 1981) or semianalytical models (Gordon et al. 1988), were in fact remarkably successful for processing and interpreting CZCS imagery, dependant as they were, on high accuracy in-water measurements of normalized water-leaving radiances, $L_{WN}(\lambda)$, and concurrently determined pigment concentrations. Any errors in the historical CZCS pigment databases are a result of the sensor measurements (radiometric accuracy and stability, as well as atmospheric correction procedures) and not a result of the algorithms employed. The NET database of water-leaving radiances and *in situ* pigment measurements, although restricted in its geographical and seasonal coverage, is still the major reliable source of data for algorithm development and is used in this paper for these reasons.

Recently, the NET database has been reworked for the SeaWiFS wavelengths and bandwidths using binomial or polynomial curve fitting procedures to generate a range of empirical algorithms, which successfully explain high percentages of the variance between the variables. All of these are completely satisfactory as SeaWiFS algorithms, and with the greater precision of the SeaWiFS sensor, they should provide accurate interpretations of the imagery (after atmospheric correction). These algorithms are listed in Table 4. Using NASA Airborne Oceanographic Lidar (AOL) data from the North Atlantic Bloom Experiment (NABE) in May 1989 (Hoge and Swift 1993) to simulate SeaWiFS data, Aiken et al. (1992) demonstrated that combinations of two-band ratios could successfully explain a greater percentage of the variance between pigment and radiance ratios than any single two-band ratio on its own (Table 5). Similar results were obtained by Aiken and Moore (1995), using data from a bio-optical model with the values for absorption and scattering coefficients taken from the literature. Algorithms for the other constituents of the water column could be derived from the same synthetic data (see Table 6).

In the following section, an attempt is made to justify the validity of band-ratio algorithms, employing simple two-band ratios or linear combinations of more than two ratios. These can account for a greater percentage of the variance between variables in the NET data, because each two-band ratio can be related to a specific property of the bio-optical assemblage, which can be demonstrated by recourse to simple bio-optical models.

Table 4. Algorithms from D. Clark.

Parameter	Case	Ratio	A_0	A_1	A_2	A_3	R^2
C_{TP}	1	$2 + 3 + 4{:}5$	8.73	-11.20	4.43	-0.62	97.0
C_{TP}	$1 + 2$	$2 + 3 + 4{:}5$	4.76	-5.36	1.70	-0.21	93.6
C_T	1	$2 + 3 + 4{:}5$	8.00	-9.99	3.77	-0.50	95.8
C_T	$1 + 2$	$2 + 3 + 4{:}5$	4.74	-5.37	1.65	-0.18	92.2
TSM	1	$2 + 3 + 4{:}5$	4.81	-7.56	3.32	-0.50	72.2
TSM	$1 + 2$	$2 + 3 + 4{:}5$	5.57	-8.64	3.83	-0.58	84.6
ISM	1	$2 + 3 + 4{:}5$	11.20	-18.70	8.77	-1.37	60.1
ISM	$1 + 2$	$2 + 3 + 4{:}5$	4.81	-7.56	3.32	-0.50	72.2
OSM	1	$2 + 3 + 4{:}5$	4.79	-8.02	3.75	-0.60	74.1
OSM	$1 + 2$	$2 + 3 + 4{:}5$	4.39	-7.29	3.35	-0.53	83.6
$c(535)$	$1 + 2$	$2 + 3 + 4{:}5$	3.56	-4.53	1.44	0.15	86.6
$c(535)$	$1 + 2$	$4{:}5$	-0.12	-1.74			81.6

Note: All are $\log_{10}$ regressions.

Table 5. AOL algorithms (Aiken et al. 1992) of the form $\alpha\big(L_u(\lambda_1){:}L_u(\lambda_2)\big)^\beta\big(L_u(\lambda_3){:}L_u(\lambda_4)\big)^\gamma$.

λ_1	λ_2	λ_3	λ_4	α	β	γ	R^2	N
410	555			0.78	-2.90		64.1	753
440	555			2.02	-2.84		86.3	753
490	555			2.51	-2.77		92.8	753
440	555	410	440	1.88	-2.47	2.71	86.8	733
440	555	440	490	2.69	-2.64	4.04	93.7	733

Table 6. Model algorithms (Aiken and Moore 1994) of the form $\alpha\big(R(\lambda_1){:}R(\lambda_2)\big)^\beta\big(R(\lambda_3){:}R(\lambda_4)\big)^\gamma$.

Algorithm	λ_1	λ_2	λ_3	λ_4	α	β	γ	R^2
Chlorophyll	412	555			1.87	-1.87		69
	443	555			1.53	-2.15		89
	490	555			1.77	-2.71		95
	443	555	412	443	0.52	-2.41	-5.20	95
	490	555	412	555	1.05	-4.66	-5.37	69
DOC	412	555			1.44	-0.92		28
	443	555			1.04	-0.56		12
	490	555			0.97	-0.51		6
	443	555	412	443	1.33	-1.10	-10.2	90
	490	555	412	555	-1.67	3.51	-14.8	77

4. BIO-OPTICAL MODELS

4.1 Analytical Basis of Band-Ratio Models

Water-leaving radiance is a function of the downwelling light field, the interface effects, and the inherent optical properties (IOPs) of the water column constituents integrated over 1–2 optical depths. Analytically, it can be expressed as

$$L_{WN} = F_0 \left[\frac{(1 - \rho)(1 - \bar{\rho})R}{n^2(1 - rR)Q} \right] \qquad (1)$$

where F_0 is the extraterrestrial irradiance, n is the refractive index of seawater, R is the irradiance reflectance, ρ is

the Fresnel reflectance at normal incidence, $\bar{\rho}$ is the Fresnel reflectance for sun and sky irradiance, r is the air-water reflectance for diffuse irradiance, and Q is the ratio of upwelling irradiance to radiance, which varies with the angular distribution of the upwelling light field, and is equal to π for an isotropic distribution. The $(1 - \rho)(1 - \bar{\rho})n^{-2}$ term gives the effect of the air-water interface, and shows a weak relationship with wavelength, varying as the refractive index of water. The term $1 - rR$ can be assumed to be unity in Case-1 waters.

Assuming the interface term is constant, the ratio of remotely sensed water-leaving radiances at wavelengths λ_i and λ_j, respectively, is expressed as

$$L_{i:j} = \frac{R(\lambda_i)Q(\lambda_j)F_0(\lambda_i)}{R(\lambda_j)Q(\lambda_i)F_0(\lambda_j)}, \qquad (2)$$

9

where the expression $L_{i:j}$ is a shorthand form for the ratio $L_{WN}(\lambda_i)/L_{WN}(\lambda_j)$.

Q shows a weak relationship with wavelength, which is analytically difficult to determine, the main factor being the relative change in scattering phase function (Morel and Gentili 1991 and 1993). The main determinant of the radiance ratio is the irradiance reflectance R. This may be expressed as

$$R(\lambda) = G(\mu_0, \lambda)\left[\frac{b_b(\lambda)}{a(\lambda)}\right], \qquad (3)$$

where $G(\mu_0, \lambda)$ represents the effect of the downwelling light field; $b_b(\lambda)$ is the backscatter coefficient; and $a(\lambda)$ the absorption coefficient. The IOPs, $a(\lambda)$ and $b_b(\lambda)$, are the sum of the optical properties of pure seawater and the optically active water column constituents, i.e., chlorophyll (a, b, and c), carotenoids, dissolved organic matter (DOM), and detrital particulates.

Substituting for R, the normalized water-leaving radiance ratio, $L_{i:j}$, is expressed as

$$L_{i:j} = g\left[\frac{a(\lambda_j)b_b(\lambda_i)F_0(\lambda_i)}{a(\lambda_i)b_b(\lambda_j)F_0(\lambda_j)}\right], \qquad (4)$$

where g is assumed to be a constant that consists of the ratios of the air-sea interface effects, the effects of the light field [the Morel and Gentili (1991) f factor], and the relative spectral variation of Q. Using Morel and Gentili's (1993) figures for the spectral variation of f/Q, g will be $1 \pm 3.5\%$ with the remotely sensed viewing geometry. For the purposes of discussion of the effects of the water constituents, the factor g has been omitted (it is assumed to be unity).

By partitioning the IOPs of the constituents of the water into the sum of the parts, $L_{i:j}$ can be expressed as

$$L_{i:j} = \frac{a_w(\lambda_j) + a_g(\lambda_j)G + a_\phi(\lambda_j)C}{a_w(\lambda_i) + a_g(\lambda_i)G + a_\phi(\lambda_i)C}$$
$$\times \frac{b_{bw}(\lambda_i) + b_{bp}(\lambda_i)P}{b_{bw}(\lambda_j) + b_{bp}(\lambda_j)P} \times \frac{F_0(\lambda_i)}{F_0(\lambda_j)}, \qquad (5)$$

where a_w and b_{bw} are the absorption and backscatter coefficients of water, respectively; P is the particulate concentration including detrital material, and b_{bp} is its specific backscatter coefficient (normally normalized to chlorophyll a concentration); G is the concentration of DOM and DOM-like absorbers and a_g its specific absorption; and C is the chlorophyll biomass concentration and a_ϕ is its specific absorption.

In this formulation, the backscatter has been decoupled from the chlorophyll concentration, and it is assumed that the relationship between the backscatter and phytoplankton biomass depends on ecological, rather than optical, correlates. The formulation of biomass absorption does not include the package effect (Duysens 1956). The

chlorophyll biomass absorption can be partitioned according to the functional groups of pigment. This includes chlorophyll a, b, and c; the photosynthetic carotenoids; and the photoprotectant carotenoids as per the following formulation:

$$Ca_\phi = a_aC_a + a_bC_b + a_cC_c,$$
$$+ a_{PS}C_{PS} + a_{PP}C_{PP} \qquad (6)$$

where C_a, C_b, C_c, a_a, a_b, and a_c are the concentrations and specific absorptions of chlorophyll a, b, and c, respectively; C_{PS}, C_{PP}, a_{PS}, and a_{PP} are the concentrations and specific absorptions of the photosynthetic and photoprotectant carotenoids, respectively.

It can be seen from this that band-ratio algorithms are almost wholly dependant on the IOPs. The CZCS algorithm, or the SeaWiFS equivalent, can be taken as a case study. The λ_i:555 nm algorithms (where $\lambda_i = 412$, 443, 490, or 510 nm) can be approximated by the following expression:

$$L_{i:j} = \frac{a_w(\lambda_j) + a_g(\lambda_j)G + a_{abc}(\lambda_j)C}{a_w(\lambda_i) + a_g(\lambda_i)G + a_{abc}(\lambda_i)C}$$
$$\times \frac{b_{bw}(\lambda_i) + b_{bp}(\lambda_i)P}{b_{bp}(\lambda_j)P} \times \frac{F_0(\lambda_i)}{F_0(\lambda_j)}. \qquad (7)$$

The particulate backscatter, b_{bp}, will come from both detrital material and phytoplankton; this backscatter, although correlated with chlorophyll biomass, shows a highly variable relationship from province to province. For all but the most oligotrophic waters, b_{bp} is greater than b_{bw} at 555 nm (or 550 nm for CZCS). Bricaud et al. (1981) show for typical oceanic particle distributions that the wavelength dependence for b_{bp} is approximately $\lambda - 1$; thus, the backscatter term in (7) can be approximated by an empirical constant.

Bricaud et al. (1981) showed for most oceanic areas, DOM absorption is correlated with chlorophyll-specific absorption, and $a_g(443)$ is approximately $0.3 \times a_\phi(443)$. If this DOM dependence is used in (7), then the radiance ratio can be approximated by

$$L_{i:j} = B_b\left[\frac{a_w(\lambda_j) + a_{g\phi}(\lambda_j)C}{a_w(\lambda_i) + a_{g\phi}(\lambda_i)C}\right]\frac{F_0(\lambda_i)}{F_0(\lambda_j)}, \qquad (8)$$

or

$$L_{i:j} = B\left[\frac{1 + CA_j}{1 + CA_i}\right], \qquad (9)$$

where B_b, B, A_j, and A_i are arbitrary constants. In the case where $L_{WN}(555)$ is the reference band of the two-band ratio and when a_g is much less than a_w (i.e., C less than $1.0\,\mathrm{mg\,m^{-3}}$), the radiance ratio can be further approximated to

$$L_{i:j} = \frac{B}{1 + CA}. \qquad (10)$$

In the analyses presented here, the hyperbolic equations (9) and (10) are the basic models for the two-band ratio algorithms that use SeaWiFS band 5 rather than the conventional model derived from a log-log fit. These hyperbolic models have the useful property that the coefficient B can be expressed in terms of the IOPs of pure seawater, i.e.,

$$B = g\left[\frac{b_{bw}(\lambda_i)}{b_{bw}(\lambda_j)}\frac{a_w(\lambda_j)}{a_w(\lambda_i)}\frac{F_0(\lambda_i)}{F_0(\lambda_j)}\right], \qquad (11)$$

and that there is a lower limit to the ratio of normalized water-leaving radiances

$$L_{i:j} = B\left[\frac{A_j}{A_i}\right] \qquad (12)$$

This lower limit is useful, since it determines the range of applicability of the algorithms, i.e., the point where the radiance ratio does not give a meaningful estimate of chlorophyll a or pigment.

The factor g in (11) corresponds to the ratio of the Morel and Gentili f/Q ratio at bands i and j. Morel and Gentili (1993) found this ratio to be 0.804 for the 440 and 565 nm wavelengths, over the whole range of water types and μ_0. Comparisons of the clear water B values in Tables 11 and 12 show the f/Q ratio to be 0.799 for the 443:555 band ratio. This further validates the hyperbolic model, since discrepancies between model values can be explained in terms of light field effects.

4.2 Model Development

Two bio-optical models were developed to support the analysis of the various algorithms: the first to determine the differential effects of the bio-optical determinands on the radiance ratios; and the second to determine the effects of the biological variability and intercorrelation of the water column constituents on the radiance ratios. The purpose of the second model was to test algorithm formulation on sets of simulated data that contained variability found in a wider range of bio-optical provinces than the NET data.

Both models use (5) and (6) with a full pigment assemblage. The package effect was not included in either model. Raman emission was included in the second model, using an approximation of Marshall and Smith's (1990) expression for surface Raman reflectance:

$$L'_{WN} = \frac{b_R E'_0}{6.0Qa + a'}, \qquad (13)$$

where E'_0 is the downwelling irradiance at the Raman excitation wavelength, b_R is the Raman scattering coefficient, a' is the absorption at the Raman excitation wavelength, and a is the absorption at the Raman emission wavelength. Without the Raman term, the model does not give a reasonable approximation to the optical properties of pure water.

4.2.1 Model Parameterization

All the data were integrated over the SeaWiFS band responses (Barnes et al. 1994). Data for pure seawater scattering were taken from Morel (1974) and for pure seawater absorbancy from Smith and Baker (1981). Particulate backscatter was scaled to the backscatter from Gordon et al. (1988), at 443 nm and 1 mg m^{-3} chlorophyll; backscatter for other wavelengths was calculated using an a^{-n} dependence, with $n = 1$. The exact value of n, however, will depend on the oceanic particle size distribution (Morel and Prieur 1977). Carder (pers. comm) indicates n depends on the $R(443):R(490)$ ratio, which is dependent on DOM and the carotenoid to chlorophyll ratio. DOM absorption was determined using a curve of the form

$$a_g(\lambda) = a_g(375)e^{-S(\lambda-375)} \qquad (14)$$

using a slope S of 0.014 and a base value of 0.06 (Bricaud et al. 1981), the slope being identical with that used in Carder et al. 1994. Detrital material was assumed to have the same basic spectral shape as DOM and was included in the model with a backscatter to absorption ratio of 1:2.18 derived from the transmission and absorption data of Prieur and Sathyendranath (1981) and assuming the San Diego harbor scattering phase function (Petzold 1972). Specific pigment absorption was taken from Bidigare et al. (1990). The model parameter values are summarized in Tables 7 and 8. The estimated global averages for pigment are shown in Table 9, and compared with data for chlorophyll specific absorption from Prieur and Sathyendranath (1981).

4.2.2 Global Determinands

This model was used to determine the differential effects of the biogeochemical parameters on the two-band ratios. The values of these parameters were fixed for a chlorophyll value of 1.0 mg m^{-3}. The pigments were fixed at the global ratios of $C_a{:}C_b$=5.77; $C_a{:}C_c$=5.01; $C_a{:}C_{PS}$=1.28; $C_a{:}C_{PP}$=5.32; determined from the global pigment data set for chlorophyll a in the range 0.8–1.2. The particulates were assumed to be phytoplankton only. The increase in scattering effectively increased the phytoplankton specific scattering. Detrital material increased scattering and the base DOM absorption in the ratio 1:2.18.

4.2.3 BSM Data

The driving variable for the Bio-Optical Synthetic Model (BSM) was chlorophyll a; in each run of the model, 2,000 random data points were generated using a log uniform random variate with values of chlorophyll from 0.018–20.08. These chlorophyll values were used to determine the detrital, DOM, and pigment concentrations, and, hence, bio-optical parameters using (6) and (7). Raman stimulated emission was simulated using a randomly varying F_0 from 60–150 μW cm^{-2} nm^{-1} using (13).

Table 7. Inherent optical properties of bio-optical constituents.

Band	λ	b_{bw}	b_{bp}	a_w	a_y	a_ϕ†	$b_R(\lambda')$
1	412	0.0034	0.0031	0.016	0.034	0.050	
2	443	0.0024	0.0030	0.015	0.023	0.058	
3	490	0.0016	0.0028	0.021	0.012	0.045	0.00048
4	510	0.0013	0.0027	0.036	0.009	0.036	0.00042
5	555	0.0009	0.0026	0.067	0.005	0.019	0.00029

† Data derived from Prieur and Sathyendranath (1981).

Table 8. Inherent optical properties of phytoplankton pigments‡.

Band	λ	a_ϕ†	a_a	a_b	a_c	a_{PS}	a_{PP}
1	412	0.050	0.017	0.003	0.021	0.008	0.022
2	443	0.058	0.018	0.013	0.046	0.019	0.045
3	490	0.045	0.003	0.011	0.011	0.036	0.049
4	510	0.036	0.001	0.001	0.002	0.033	0.022
5	555	0.019	0.001	0.002	0.003	0.008	0.001

† Data derived from Prieur and Sathyendranath (1981).
‡ Data derived from Bidigare et al. (1991).

Table 9. Inherent optical properties of phytoplankton pigments weighted according to climatological ratios‡.

Band	λ	a_ϕ†	a_Σ§	a_a	a_b	a_c	a_{PS}	a_{PP}
1	412	0.050	0.032	0.017	0.001	0.004	0.006	0.004
2	443	0.058	0.053	0.018	0.003	0.009	0.015	0.008
3	490	0.045	0.046	0.003	0.002	0.002	0.030	0.009
4	510	0.036	0.032	0.001	0.000	0.000	0.027	0.004
5	555	0.019	0.009	0.001	0.000	0.001	0.007	0.000

† Data derived from Prieur and Sathyendranath (1981).

‡ The absorbance values are calculated according to climatological ratios ($C_a{:}C_b{=}5.77$, $C_a{:}C_c{=}5.01$, $C_a{:}C_{PS}{=}1.28$, and $C_a{:}C_{PP}{=}5.32$). The data is from the GIN Seas, EqPac, NEAT, and the Antarctic.

§ $a_\Sigma = a_a + a_b + a_c + a_{PS} + a_{PP}$.

The variance for the scattering was derived from the UK-BOFS database using $c(670)$ and chlorophyll, for data at or above the 10% light level. The variance of the $c(670)$ to chlorophyll ratio was found to be log-normally distributed with a variance of 0.823; since log variance is scale invariate, this log variance was used to generate the detrital backscatter contribution. The variance for phytoplankton backscatter was arbitrarily set at 0.100. The ratio of detrital backscatter was twice the value of phytoplankton backscatter; this figure was derived from Prieur and Sathyendranath's (1981) $b_{min}(525)$. The pigment data was similarly found to be log-normally distributed, with variances of 1.017, 0.683, 0.482, and 0.151 for chlorophyll b, chlorophyll c, PSC, and PPC, respectively.

The variation of DOM absorption with chlorophyll is dependant on oceanic conditions. Bricaud et al. (1981) observe an almost constant background, $a_g(375) = 0.06$, whereas Prieur and Sathyendranath (1981) and Carder et al. (1989) show a weak correlation with chlorophyll a, and Carder et al. (1986) show a good relationship with chlorophyll a. The assumption applied here is that a_g co-varies with chlorophyll a, but with a log variance of 0.21, derived from NABE DOM concentrations. The relationships described above resulted in the 95% ranges in the model input data of 0.023–15.02 for chlorophyll a; 0.001–1.70 for chlorophyll b; 0.002–1.87 for chlorophyll c; 0.015–9.69 for PSC; 0.003–5.20 for PPC; and 0.024–13.62 for DOM relative absorption.

In order to compare the results from the BSM data with the NET data, it was necessary to simulate pigment data. Trees et al. (1985) showed that the fluorometric method (Yentsch and Menzel 1963) of chlorophyll a determination was affected by coexisting chlorophyll b and c. Using the following figures, derived from Trees et al. (1985), and validated by comparison with NEAT HPLC data, fluorometric chlorophyll a was calculated as

$$C_S = 0.941C_a - 0.292C_b + 0.371C_c \qquad (15)$$

and pigment as

$$P_S = 1.166C_a + 0.616C_b + 0.544C_c. \qquad (16)$$

5. DATA ANALYSES

5.1 Algorithm Development

In the previous section, a theoretical basis for band-ratio algorithms using standard hydrological, bio-optical models was established. In this section, these models are used with selected data sets to derive empirical fits of the data to produce the algorithms for SeaWiFS. The inherent statistical properties of the NET data are explored to establish a baseline for comparative reference. Using the conventional power law model and the pigment definition for the CZCS algorithms

$$C_a + C_P = \alpha' \left(L_{i:j} \right)^{\beta'} \qquad (17)$$

or

$$\ln \left(C_a + C_P \right) = \ln(\alpha') + \beta' \ln \left(L_{i:j} \right). \qquad (18)$$

Table 10 shows the coefficients of the ln-ln regression and the percentage of variance explained (R^2) for pigment ($C_a + C_P$) regressed against all two-band combinations for the NET data (SeaWiFS band set), and Fig. 6 shows the scatterplots for the major ratios. The regressions fall into four groups, which depend on the wavelength of the reference radiance. The first group, reference $L_{WN}(555)$, shows very high R^2 values for all two-band ratios, indicating that $C_a + C_P$ is highly correlated in all cases. The increasing value of R^2 from 412 to 443 to 490 to 510 is surprising since the 490 and 510 bands are at longer wavelengths than the chlorophyll a (or phaeopigment) absorption peaks. This is due to the highly correlated co-occurrence and co-variance of chlorophyll and carotenoids (which absorb at 490 and 510 nm), demonstrated in Section 2, which means carotenoids effectively and accurately behave as surrogates for chlorophyll at the longer wavelengths. Coupled with this effect, the longer wavelengths are least affected by the absorption of light in the blue spectral region by DOM, which contaminates the 412 and 443 nm wavebands to the maximum extent. The second and third groups of band ratios (reference bands 510 and 490 nm, respectively) also show increasing R^2 values with increasing wavelength, 412 to 443 to 490 nm. The same explanations of the effects of co-existing DOM and accessory pigments (carotenoids) apply. In each case, the percentage of variance explained is smaller than for the first group as the reference wavelengths are influenced somewhat more by carotenoid absorption.

Only the $L_{WN}(412){:}L_{WN}(443)$ ratio is poorly correlated with pigment; (this is understandable since these wavebands are influenced most significantly by the absorption of DOM and detritus which have similar absorption spectra). Table 10 shows the ln-ln regression coefficients and R^2 values for the BSM data set. The scatterplots for the $L_{WN}(555)$ base ratios compared to NET data are shown in Fig. 7. Interestingly, these regressions show exactly the same patterns of coefficients and R^2 values for the

four groups of band ratios as the NET data (Table 10). The R^2 values are considerably higher for the BSM data (up to 96%) where the only source of variability is from the bio-optical determinands. The higher R^2 values are explained by the fact that no measurement error was added to the BSM data. The inference from this observation is that since the synthetic pigment and radiance data are so highly correlated, the basic bio-optical model used in the synthesis and the parameter values employed are both reliable.

Using simple bio-optical models, a hyperbolic function of chlorophyll was found to be the simplest expression for the relationship for the band ratio, see (10), with an asymptotic coefficient (B) as $C \to 0$, which relates to the IOPs of pure water given by (11). This simpler model is only robust where chlorophyll is low, and can be used to empirically determine the clear water B. Using the clear water B, the full range of data (Case-1 and Case-2) can be fitted using the full model (9). Tables 11 and 12 show the coefficients for the full model with $C_a + C_P$ and C_a and band ratios fitted for the NET data. Tables 13 and 14 show the coefficients for chlorophyll a and simulated pigment for the BSM data. In all cases, the percentage of variance explained is high, up to 91% for the NET data and up to 96% for the key band ratios for the BSM data. In all cases, this model provides a superior fit compared with the ln-ln regressions.

Again, the primary conclusion from these findings is the basic bio-optical models and parameters used are sound, as demonstrated by their utility to generate relationships with high confidence. A secondary conclusion is that these methods, using synthetic data, are suitable for the generation of algorithms for parameters where there are few *in situ* calibration measurements, but where there is a good knowledge of the IOPs of the parameters (e.g., DOM, pigments, etc.). It is suggested here that good *in situ* data sets with a limited range of parameter values (e.g., NET data which has no accessory pigment measurements) can be *bootstrapped* to synthetic data to infer a greater number of parameters. It can be shown in these and other analyses that there is potential for closure between apparent optical measurements and synthetic measurements that use IOPs.

5.2 Sensitivity Analysis of Ratio Models

Figure 8 shows the sensitivity of retrieved pigment concentration for each of the primary ratios (412:555, 443:555, 490:555, and 510:555). Table 15 shows symbolically the effects on the remaining secondary band ratios, together with the main ratios. At the level of chlorophyll a considered, detritus, DOM, and chlorophyll-specific scattering all change the apparent chlorophyll retrieved and the ratios by 5–10%, the effect being greatest in the blue part of the spectrum and decreasing towards the green. It is surprising that scattering should depress the ratio and result in an

Table 10. Log regressions of NET and synthetic simulated pigments with band ratios.

Band Ratio	NET $C_a + C_P$			BSM P_S		
	Intercept	Slope	R^2	Intercept	Slope	R^2
412:555	−0.339	−1.095	72.2	−0.199	−1.387	90.9
443:555	0.051	−1.284	81.7	0.028	−1.562	95.1
490:555	0.696	−2.085	86.4	0.322	−2.262	95.4
510:555	0.688	−2.864	86.8	0.151	−3.541	95.9
412:510	−0.505	−1.533	58.7	−0.418	−2.193	84.4
443:510	−0.464	−2.209	74.4	−0.073	−2.702	87.8
490:510	0.627	−7.035	81.5	0.604	−6.117	92.3
412:490	−0.791	−1.733	46.5	−0.967	−3.315	77.5
443:490	−0.924	−2.983	65.9	−0.605	−4.745	82.6
412:443	−0.601	−2.913	20.9	−1.629	−9.761	58.2

Table 11. NET data pigment curve fits.

Band Ratio	C	A_1	A_2	R^2	C_w†
412:555	13.14 ± 1.86	0.059 ± 0.07	16.79 ± 0.76	84.4	13.80
443:555	9.55 ± 1.08	0.068 ± 0.05	9.68 ± 0.40	87.9	11.94
490:555	5.29 ± 0.37	0.232 ± 0.04	3.82 ± 0.16	89.8	5.67
510:555	3.07 ± 0.15	0.262 ± 0.03	1.94 ± 0.09	91.4	2.80

† C_w adjusted for Raman scattering in model.

Table 12. NET data chlorophyll curve fits.

Band Ratio	C	A_1	A_2	R^2	C_w†
412:555	13.14 ± 1.86	0.081 ± 0.09	20.51 ± 0.94	83.3	13.80
443:555	9.55 ± 1.08	0.115 ± 0.07	11.04 ± 0.52	86.5	11.94
490:555	5.29 ± 0.37	0.328 ± 0.05	4.27 ± 0.21	88.5	5.67
510:555	3.07 ± 0.15	0.350 ± 0.04	2.44 ± 0.12	90.5	2.80

† C_w adjusted for Raman scattering in model.

Table 13. BSM chlorophyll a curve fits.

Band Ratio	C	A_1	A_2	R^2	C_w†
412:555	13.82 ± 0.84	0.167 ± 0.03	23.09 ± 0.34	90.3	13.80
443:555	11.74 ± 0.52	0.279 ± 0.03	18.58 ± 0.24	92.7	11.94
490:555	5.35 ± 0.10	0.499 ± 0.02	7.42 ± 0.09	95.4	5.67
510:555	2.63 ± 0.02	0.662 ± 0.01	3.61 ± 0.04	95.8	2.80

† C_w adjusted for Raman scattering in model.

Table 14. BSM pigment curve fits.

Band Ratio	C	A_1	A_2	R^2	C_w†
412:555	13.82 ± 0.84	0.134 ± 0.03	17.74 ± 0.26	90.0	13.80
443:555	11.74 ± 0.52	0.219 ± 0.02	14.26 ± 0.19	92.6	11.94
490:555	5.35 ± 0.10	0.385 ± 0.01	5.69 ± 0.07	95.2	5.67
510:555	2.63 ± 0.02	0.510 ± 0.01	$2..76 \pm 0.03$	95.6	2.80

† C_w adjusted for Raman scattering in model.
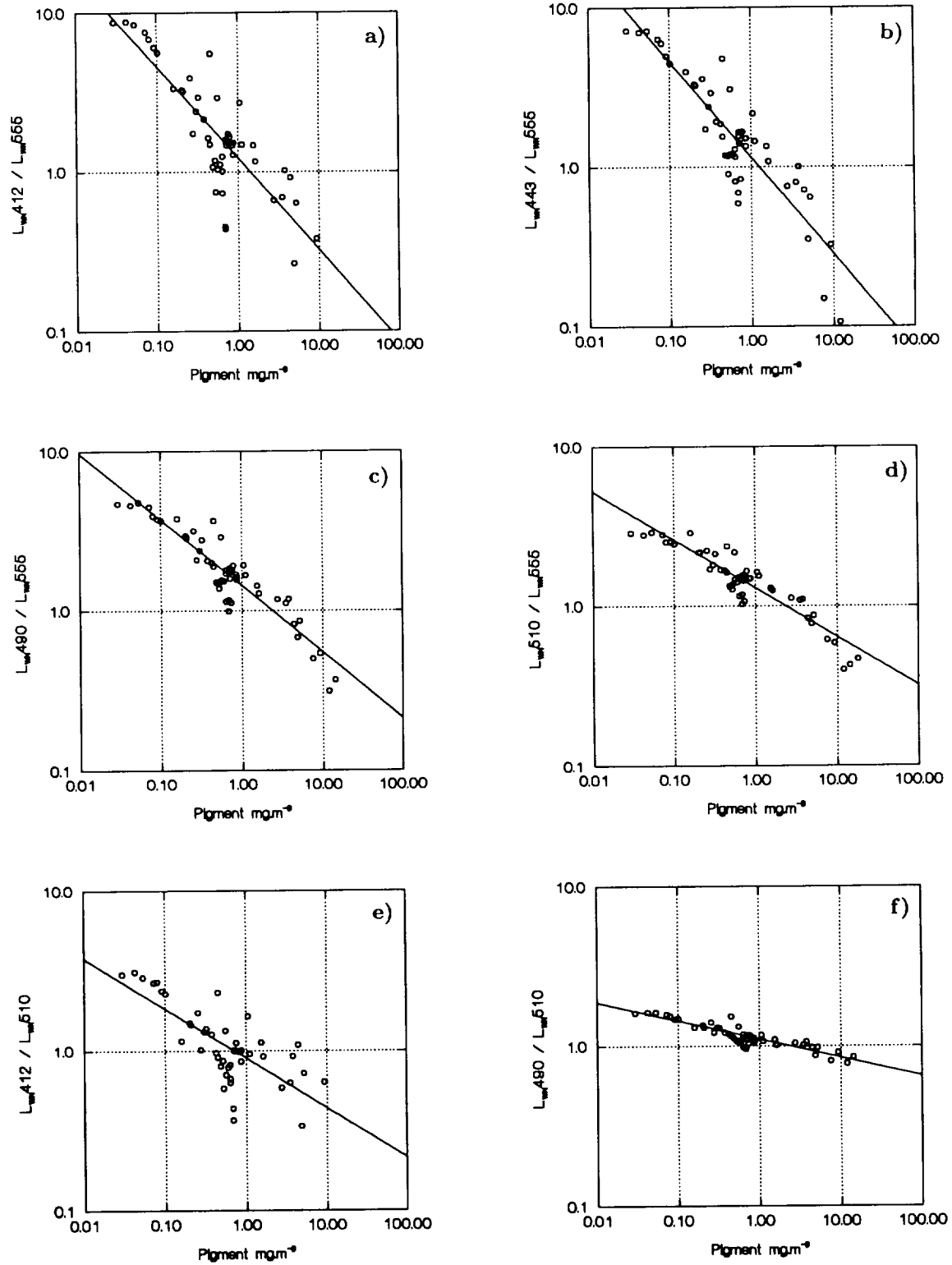
Fig. 6. NET data (weighted pigment) scatterplots: **a)** $L_{WN}(412){:}L_{WN}(555)$, **b)** $L_{WN}(443){:}L_{WN}(555)$, **c)** $L_{WN}(490){:}L_{WN}(555)$, **d)** $L_{WN}(510){:}L_{WN}(555)$, **e)** $L_{WN}(412){:}L_{WN}(510)$, and **f)** $L_{WN}(490){:}L_{WN}(510)$.
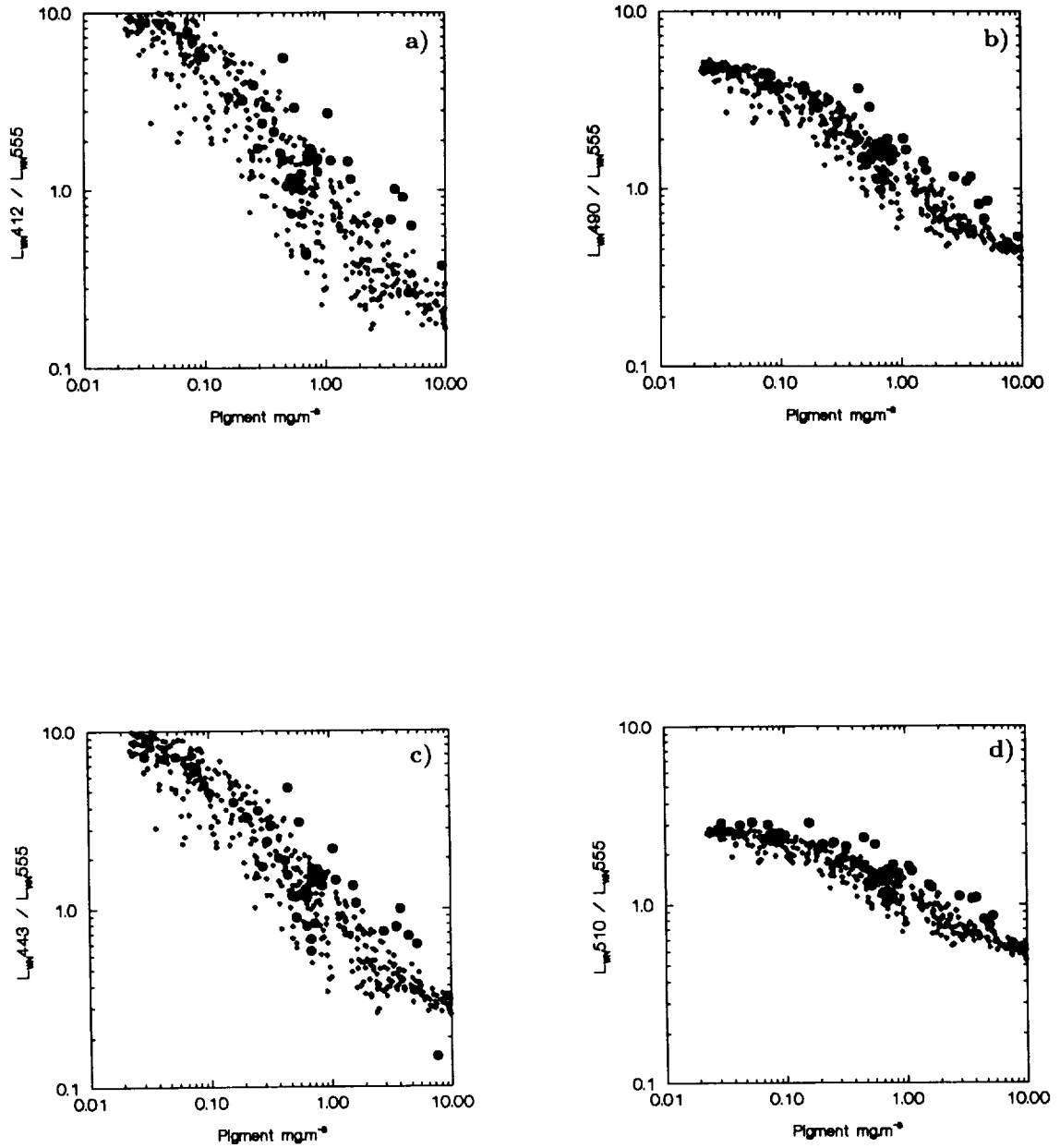
Fig. 7. NET data (circles) compared with the synthetic data set (diamonds): **a)** $L_{WN}(412){:}L_{WN}(555)$, **b)** $L_{WN}(490){:}L_{WN}(555)$, **c)** $L_{WN}(443){:}L_{WN}(555)$, and **d)** $L_{WN}(510){:}L_{WN}(555)$.
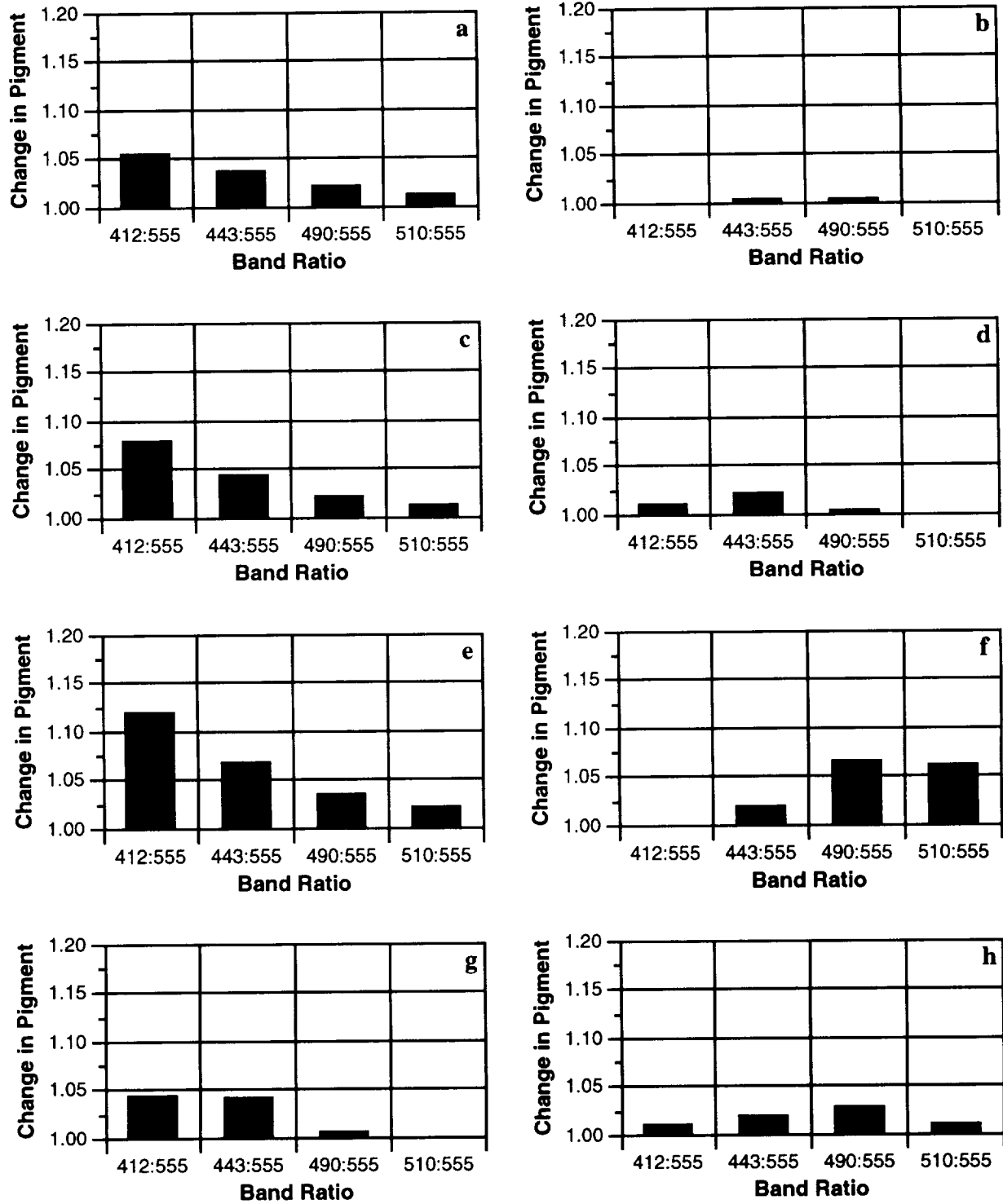
Fig. 8. The effects on retrieved pigment of 20% (10% for detritus) change in concentration relative to a climatoligical value: a) scattering, b) C_b, c) DOM, d) C_c, e) detritus, f) C_{PS}, g) C_a, and h) C_{PP}. All values are calculated for a chlorophyll concentration of $1.0\,\mathrm{mg\,m^{-3}}$.

Table 15. Sensitivity of ratio to model single parameter change.

Band Ratio	Scat.	Gelb.	Detr.	Chl. a	Chl. b	Chl. c	PSC	PPC
412:555	++	++++	++++	++				
443:555	++	++	+++	++		+	+	+
490:555	+	+	++				+++	+
510:555			+				+++	
412:443	+	++	+++++					
443:490		+	++++	++		+		
490:510			+++				--	
412:490	+	+++	+++++	++			---	
443:510	+	+	+++++	++		+	--	
412:510	++	+++	+++++	++			---	

Note: $< 3\%$ +; $3 - -5\%$ ++; $5 - -7\%$ +++; $7 - -20\%$ ++++; $> 20\%$ +++++ (and similarly for negative values).

Table 16. Principal component factor loadings.

Band Ratio	F_1–NET	F_1–BSM	F_2–NET	F_2–BSM	F_3–NET	F_3–BSM
412:555	+	+			+	--
443:555	++	++			++	
490:555	+++	+++	--	-	+	----
510:555	+++	++++	--	--	+++++	-----
412:443	----	---	+++++	+++++	-	-----
443:490		--	+		+++	+++++
490:510	++	+	--	--	-----	++++
412:490	+	--	+++	+++	+	++
443:510	-				--	+++++
412:510		--	++		--	+++

Note: $< 3\%$ +; $3 - -5\%$ ++; $5 - -7\%$ +++; $7 - -20\%$ ++++; $> 20\%$ +++++ (and similarly for negative values).

increase in apparent chlorophyll retrieved, but it should be remembered that the ratios have been explored in a region where backscatter from water is dominant.

Chlorophyll a has a dominant effect on the 412:555 and 443:555 ratios, contrasted with photosynthetic carotenoids which affect the 490:555 and 510:555 ratios. The photoprotectant carotenoids effect most of the band ratios with the dominant affect being on the 490:555 ratio. Chlorophylls b and c have only minor affects on the band ratios, and major province difference would be needed for their affect on band ratios to become important. The only two-band ratios affected by all pigments are the 443:555 and 490:555, with the later being less affected by DOM or detritus.

Of all the secondary ratios, the most useful may be 412:443, which is not influenced by pigment but is strongly influenced by DOM and detritus. For determining accessory pigments, the 412:490, 443:510, and 412:510 ratios seem most promising, since they show a differential influence between photosynthetic carotenoids and chlorophyll a. The response of the different ratios to differing biogeochemistry, would imply that most, if not all, of the optical and biogeochemical information found in upwelled spectra is contained in the primary and secondary ratios considered in this study.

5.3 Analysis of NET and BSM Data

The NET data represent high quality optical data, with limited measures of biogeochemical parameters other than chlorophyll a and phaeopigment. In order to determine the bio-optical variability of the data, principal components analysis was used, and the results were compared with the BSM data set containing variability from a wider range of provinces than those present in the NET data. The aim was to determine if the NET data contained sufficient variability to generate global algorithms, and to determine how far bio-optical variability reflects ecosystem variability.

Analysis of the NET data log radiance ratios, by principal components analysis using varimax rotation, showed that three factors could be extracted explaining 99.6% of the total variance. These three factors explained 57.5, 41.2, and 0.9 percent of the variance, respectively. The relative factor loadings are shown in Table 16, with the normalized factor loadings for the $L_{WN}(555)$ based ratios shown in Fig. 9. The first column of each factor pair shows the factor pattern for the NET data. By comparison with the previous analysis of radiance ratio patterns, the first two factors, F_1 and F_2, can be ascribed to pigment biomass and detritus concentration, respectively, with the first factor
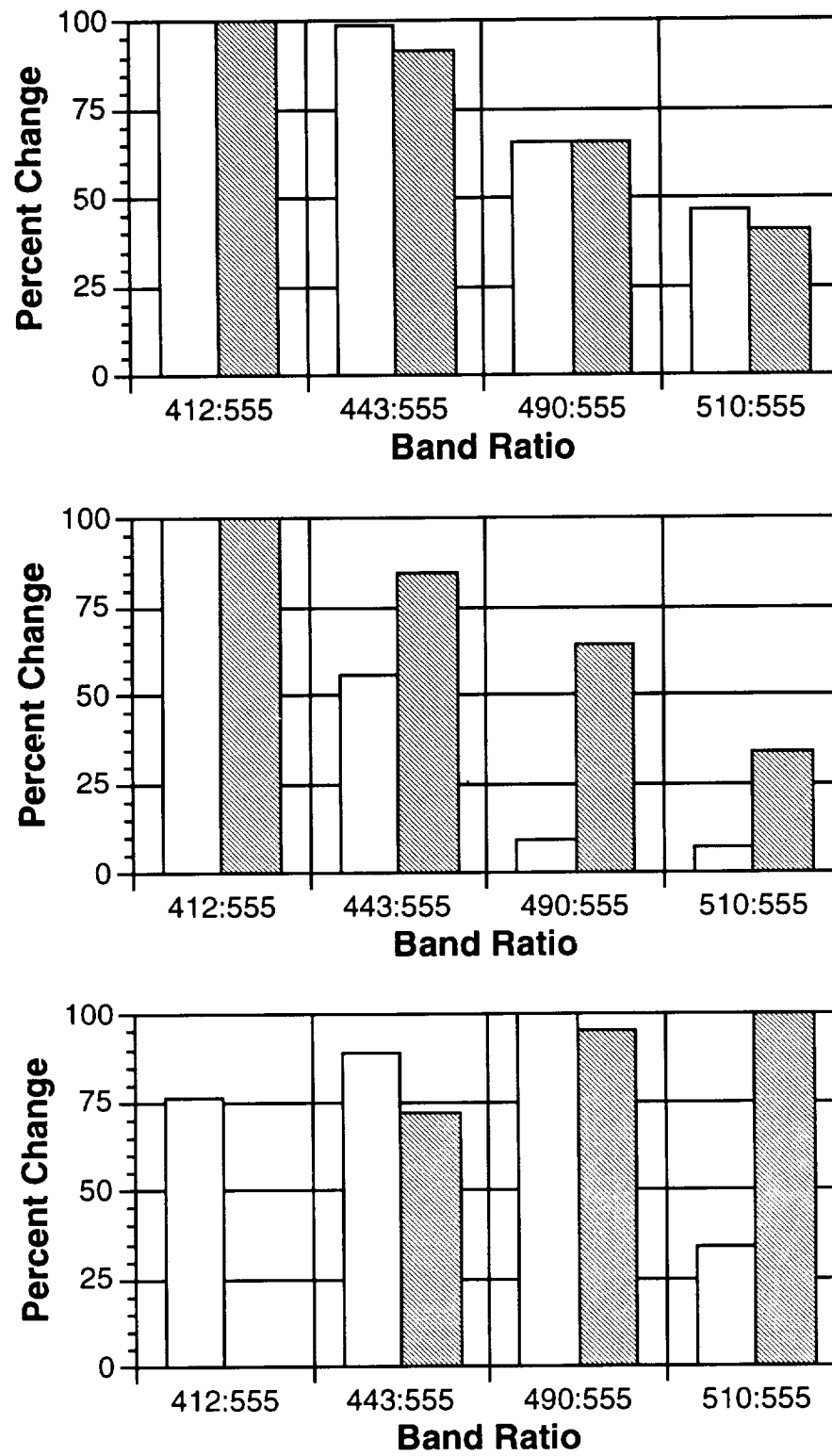
Fig. 9. The normalized spectral change in the factors F_1 (top), F_2 (middle), and F_3 (bottom). The NET data is shown as the white bars and the simulated data as the hatched bars.

showing a high correlation with log pigment $(R^2 \dot{=} 89.5\%)$ or log chlorophyll $(R^2=89.2\%)$. The meaning of the third factor, F_3, is more difficult to determine, but the principal loadings are on those ratios which correlate with carotenoid concentration, notably 490:510 and 510:555. This factor could be related to absolute carotenoid concentration or relative pigment abundance (PSC:PPC ratio).

The BSM data showed a similar factor pattern to the NET data with 99.9% of the total variance explained, and the three factors explaining 52.3%, 43.2%, and 4.4% of the variance, respectively. The change in the total variance explained is probably attributable to the BSM data assuming a perfect radiometer; the relatively small change in total variance explained indicates the quality of the NET optical data. The higher percentage variance explained by the third factor, reflects the greater range of pigment and detrital variance introduced into the synthetic data. The factor profiles are shown in Table 16, and the patterns for F_1 and F_2 are almost identical to the NET data. The comparison with F_3, is less clear, but both NET and BSM data show loadings on ratios that relate to carotenoid concentration. The difference in the precise loadings of the third factor is likely to be caused by the lower pigment variability in the NET data compared with the BSM data. This hypothesis needs to be tested further using data sets that have concurrent radiance measurements and HPLC pigments. These will become available as part of the SeaWiFS calibration and validation activity.

In the BSM data, the underlying biogeochemistry is known a priori; thus, the factors can be related to their principal driving variable. F_1 shows the best relationship with total pigment, chlorophyll $(a,\ b,\ \text{and}\ c)$, and carotenoids, with the best correlation being with total pigment $(R^2=89.9\%)$. F_2 shows little correlation with pigment, correlating with the total particulate concentration and total DOM-like absorbance (i.e., detrital absorbance), but with a poor R^2 of 58.1% and 62.3%, respectively. F_3 shows low correlations with all variables, the best being with DOM-like absorbance and photosynthetic carotenoids, with R^2 of 30.6% and 27.6% respectively. This would still seem to indicate F_3 represents the chlorophyll to carotenoid ratio, since an increase in DOM has almost the same effect on a normalized SeaWiFS spectrum as an increase in carotenoids.

Figure 9 shows the spectral differences in the factors, derived by selecting data where each factor was lower than the factor average. F_1 and F_2 show similar patterns in both the NET data and the BSM data, although for F_2 the typical DOM curve is more pronounced in the NET data than in the BSM data. F_3 shows a greater disparity between the NET data and the BSM data; the main affect in the NET data is the 490:555 ratio whereas in the BSM data, it is the 510:555 ratio. The spectral patterning of the change in the NET data would suggest a shift in PPC, compared with a shift in total carotenoid in the BSM data. The change in PPC is probably due to light adaptation in

the NET data, a factor that was not included in the model. Figure 5i shows such a shift in pigment ratios; high light areas, e.g., EqPac and BATS, show a higher PPC relative to PSC ratio or PPC to carotenoid ratio.

It is surprising that the information in the NET and BSM data sets can be reduced to three factors, whereas there are five factors in the biogeochemical variables that generate the BSM optical data. This may be due to the limited range of bands chosen, but the reduction of optical data to three factors is supported by a number of other studies. Sathyendranath (1981), using principal components analysis on log reflectance data from 400–650 nm with a resolution of 10 nm, found three factors explaining 57.6%, 42.1%, and 0.2%, respectively, of the variance. Garver et al. (1995), using empirical orthogonal factor analysis on absorbance spectra from 400–700 nm, found detrital and phytoplankton components explaining 54% and 44%, respectively, of the variance; the residual 2% of variance was assumed to be pigment variability. Mueller (1976), using principal components analysis on airborne spectrometer data from 400–750 nm with a resolution of 5–7.5 nm, found four factors explaining 77.6%, 17.21%, 2.4%, and 0.9%, respectively, of the variances; the first three factors were related to pigment, showing similar patterns to the NET factors, but the fourth factor was unrelated to pigment and may have been due to residual atmospheric effects.

From this and other studies, it can be concluded that for oceanic waters, the SeaWiFS band set provides sufficient information to adequately specify the upwelling spectrum, and that the full compliment of ratios contain the full variance of the original upwelling radiance. The total variability in the optical signal can be reduced to three factors, although there are more factors in the underlying biogeochemistry. This fact has two implications for algorithm development: first, it is unlikely that more than three suitably chosen ratios are needed to retrieve any parameter to maximum accuracy; and second, different biogeochemical signals are not uniquely converted to optical signatures, implying that the perfect single biogeochemical parameter algorithm may not exist.

5.4 Multiband Algorithms

Multiband algorithms were developed using two methodologies, the first used empirical multiple regression of log ratios to log pigment, i.e., fitting curves of the form

$$\ln(C_a + C_P) = \alpha_0 + \alpha_1 \ln(L_{i:j}) + \alpha_2 \ln(L_{m:n}) \tag{19}$$

which is equivalent to

$$C_a + C_P = a \prod_{i}^{k} \left[\frac{L_{i:j}(k_1)}{L_{i:j}(k_2)} \right]^{b(k)}, \tag{20}$$

where k represents an index to two vectors of band ratios k_1 and k_2. The second method used linear combinations of the hyperbolic estimates. Before examining these algorithms, it is appropriate to make a statistical comment. First, the R^2 values returned by multiple log regression are not comparable with those returned by either nonlinear curve fitting or by *linear* multiple regression. Second, a small improvement in R^2 can be obtained by shifting the position of one outlier, and may not be a real improvement in the quality of calibration. With these caveats in mind, log-log multiple regressions are considered hereafter.

Table 17 shows multiple regression algorithms for the NET data. The best R^2 achieved is 87.3% (for the 443:490 and 443:555 combination), which represents a marginal improvement of the variance explained compared with 86.8% (510:555 in Table 10). Compared to the R^2 for the 443:555 ratio, however, an improvement of 6.6% is achieved. Figure 10a shows comparison of this algorithm with the single ratio hyperbolic model; the difference between the two are slight, but a few points are pulled closer to the 1:1 line. The robustness of this algorithm was tested with some data collected in the Antarctic (BOFS Sterna), where there are known differences in the optical properties of the water (Mitchell and Holm-Hansen 1991 and Sullivan et al. 1993).

Figure 10b shows a comparison between the NASA CZCS chlorophyll algorithm and the multiple regression algorithm. The retrieval shows a less biased estimate of chlorophyll than the NASA algorithm, with a slope closer to 1:1. The retrieval is noisier, and this may be due to radiometric problems, since the noise is additive and increases as more bands are used. It is not known if this will be a problem for SeaWiFS. It is noteworthy that a retrieval developed on one data set, should show an improvement with another from a different bio-optical province.

Table 18 shows the algorithms developed from the BSM data, with the R^2 being in the range 93.3–98.1%. Since the synthetic model assumes no error in measurements, these are the best retrievals to be expected unless Raman emission is modeled. The difference between these R^2 and the NET data R^2 is best explained by the pigment analysis methodology, since an error of 5–10% is expected in the Yentsch and Menzel (1963) chlorophyll. Table 18 also provides a list of algorithms for new biogeochemical variables that may be tested when data sets with more extensive sea-truth measurements than the NET data become available.

Table 19 shows a test of multiple regression algorithms restricted to the SeaWiFS bands which are compatible with the CZCS. Except for total pigment, no improvement could be found taking a band combination. The list demonstrates the alternative interpretations that can be derived from CZCS imagery; in particular it emphasizes the fact the 510:555 ratio is a carotenoid retrieval.

Multiple regression is a more appropriate technique for the hyperbolic estimates, since the estimates of pigment or chlorophyll are linear. Such algorithms are more attractive since the intermediate estimates can be interpreted in terms of pigment. Table 20 gives the results of linear combinations of pairs of estimates. In all cases, except the 443:555 and 510:555 combination, there was no significant intercept for the regression. The best retrieval was for the 443:555 and 490:555 combination, with an R^2 of 95.3%; this algorithm is shown in Fig. 11a, compared with the 443:555 hyperbolic fit. Compared with the ln-ln multiple regression in Fig. 10a, there is less bias at low pigment concentrations, whilst retaining the 1:1 relationship at high pigment concentrations. The results for the Antarctic data shown in Fig. 11b are encouraging, with points pulled closer to the 1:1 line; however, there may be a slight tendancy to overestimate pigment in this data. The 443:555 and 490:555 combination has advantages for implementation as a remotely sensed algorithm; it avoids the 412 nm band where atmospheric correction may be a problem, and tends to the 490:555 algorithm in high pigment waters where $L_{WN}(443)$ tends toward zero.

6. IMPLEMENTATION

The algorithms shown in the previous sections are all valid for the data and models considered. The development on an interim CZCS compatible algorithm involves consideration of the sensor aspects and state-of-the-art atmospheric correction. The data to be obtained from the SeaWiFS instrument is different from modeled and sea-truth data in three important aspects:

1) The data is digitized on a limited scale—10 bits at the top of the atmosphere compared with 16 bit resolution for the NET data and infinite resolution for the model data;

2) Atmospheric attenuation of the water-leaving signal will reduce the effective level still further, especially at the shorter wavelengths, i.e., bands 1 and 2; and

3) The model and NET data are both based on nadir viewing geometry, whereas the SeaWiFS instrument will view up to 58.3° off nadir.

To address the first two points, digitization of the data has been simulated by assuming a sun angle of 50° and an atmospheric transmission of 0.5. This assumption results in a dynamic range of about 160 counts for the water-leaving radiance, and corresponds to fairly high atmospheric turbidity in the early spring, e.g., the North Atlantic bloom. Figure 12 shows the mean water-leaving radiance for bands 1–4, compared with pigment averaged into log ranges. For bands 1 and 2, there is no detectible water-leaving radiance above $10\,\mathrm{mg\,m^{-3}}$, compared to bands 3 and 4 where there is significant water-leaving radiance. The issue of viewing angle can only be addressed theoretically at present, since there are limited data, e.g., Polarization and Directionality of the Earth's Reflectances

Table 17. NET data log multiple regression algorithms.

Variable	Constant	Coeff. 1	Ratio 1	Coeff. 2	Ratio 2	R^2
C_a	0.45	1.57	412:510	−2.46	443:555	84.7
C_a	0.94	3.47	443:490	−2.58	443:555	86.4
$C_a + C_P$	0.59	1.48	412:510	−2.41	443:555	85.4
$C_a + C_P$	1.09	3.39	443:490	−2.55	443:555	87.3

Table 18. BSM data log multiple regression algorithms.

Variable	Constant	Coeff. 1	Ratio 1	Coeff. 2	Ratio 2	Coeff. 3	Ratio 3	R^2
C_S	−0.040	4.60	412:510	−7.22	443:555	3.46	490:555	97.2
C_S	0.345	4.60	443:490	−2.89	443:555			96.1
P_S	0.194	4.99	412:510	−7.98	443:555	4.16	490:555	94.2
P	0.918	2.64	443:510	−2.77	412:555			97.7
P	0.229	10.77	490:510	−4.58	443:555			98.1
G	0.616	2.44	412:443	−4.43	412:555	11.12	490:510	98.2
G	0.657	12.49	412:510	−12.50	443:555			97.7
$C_{PP} + C_{PS}$	−0.133	3.93	412:443	−1.55	443:490	−3.71	510:555	97.1
$C_{PP} + C_{PS}$	−0.174	0.61	443:490	−3.91	510:555			95.9
DOM	−0.012	4.69	412:443	−1.41	412:490	−3.61	510:555	98.6
DOM	−0.021	0.39	443:490	−3.77	510:555			94.7
C_{abc}	0.724	0.58	412:443	−2.32	490:555			93.3
C_{TP}	1.063	−2.24	490:555					93.3

Table 19. BSM data CZCS compatible log multiple regression algorithms.

Variable	Constant	Coeff. 1	Ratio 1	Coeff. 2	Ratio 2	R^2
C_a	−0.157	−1.59	443:555			93.3
P_S	0.113	−1.60	443:555			93.2
P	1.024	−1.69	443:555			96.7
$C_{PP} + C_{PS}$	−0.251	−3.55	510:555			95.7
G	1.579	−1.70	443:555			93.2
DOM	−0.069	−3.54	443:555			94.2
C_{TP}	13.920	−40.60	510:555	20.76	553:510	92.7

Table 20. NET data multiple regression hyperbolic fit pigment.

Constant	$H(\lambda_1{:}555)$	Coeff. 1	$H(\lambda_2{:}555)$	Coeff. 2	R^2
	412	0.188 ± 0.03	443	1.188 ± 0.08	84.8
	412	0.519 ± 0.15	490	1.121 ± 0.05	92.5
	412	0.954 ± 0.07	510	0.759 ± 0.04	91.4
	443	−0.461 ± 0.03	490	1.821 ± 0.08	95.3
0.757 ± 0.24	443	−0.659 ± 0.02	510	1.101 ± 0.29	66.0
	490	1.903 ± 0.13	510	−0.653 ± 0.06	91.6
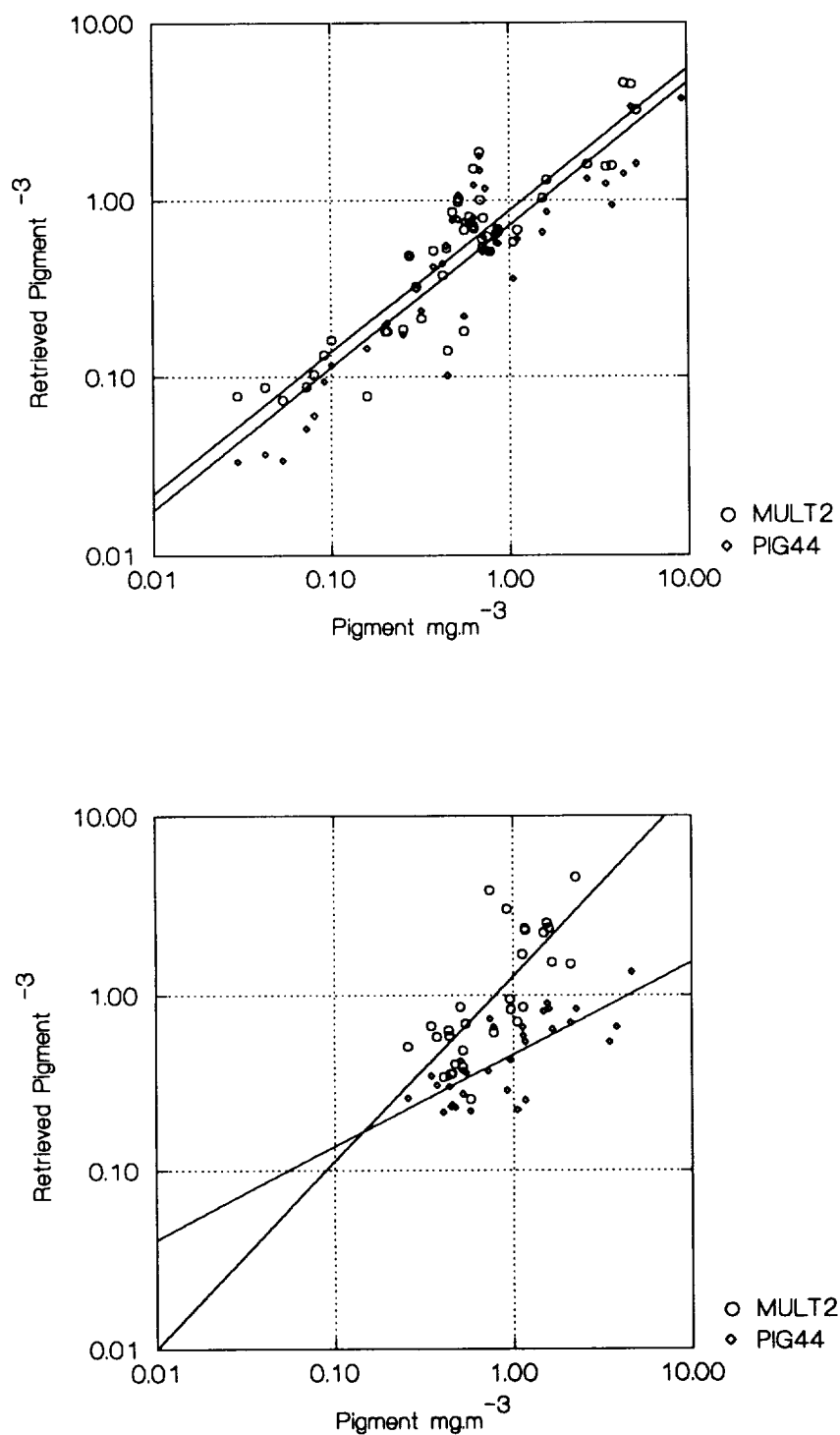
Fig. 10. Multiple regression log-log pigment $[\ln(C_a + C_P) = 0.59 + 1.48\ln(L_{WN}(412){:}L_{WN}(510)) - 2.41\ln(L_{WN}(443){:}L_{WN}(555))]$ (circles and upper line) compared with hyperbolic pigment $H(443{:}555)$ (diamonds and lower line): **a)** NET data (top) and **b)** Sterna data (bottom).
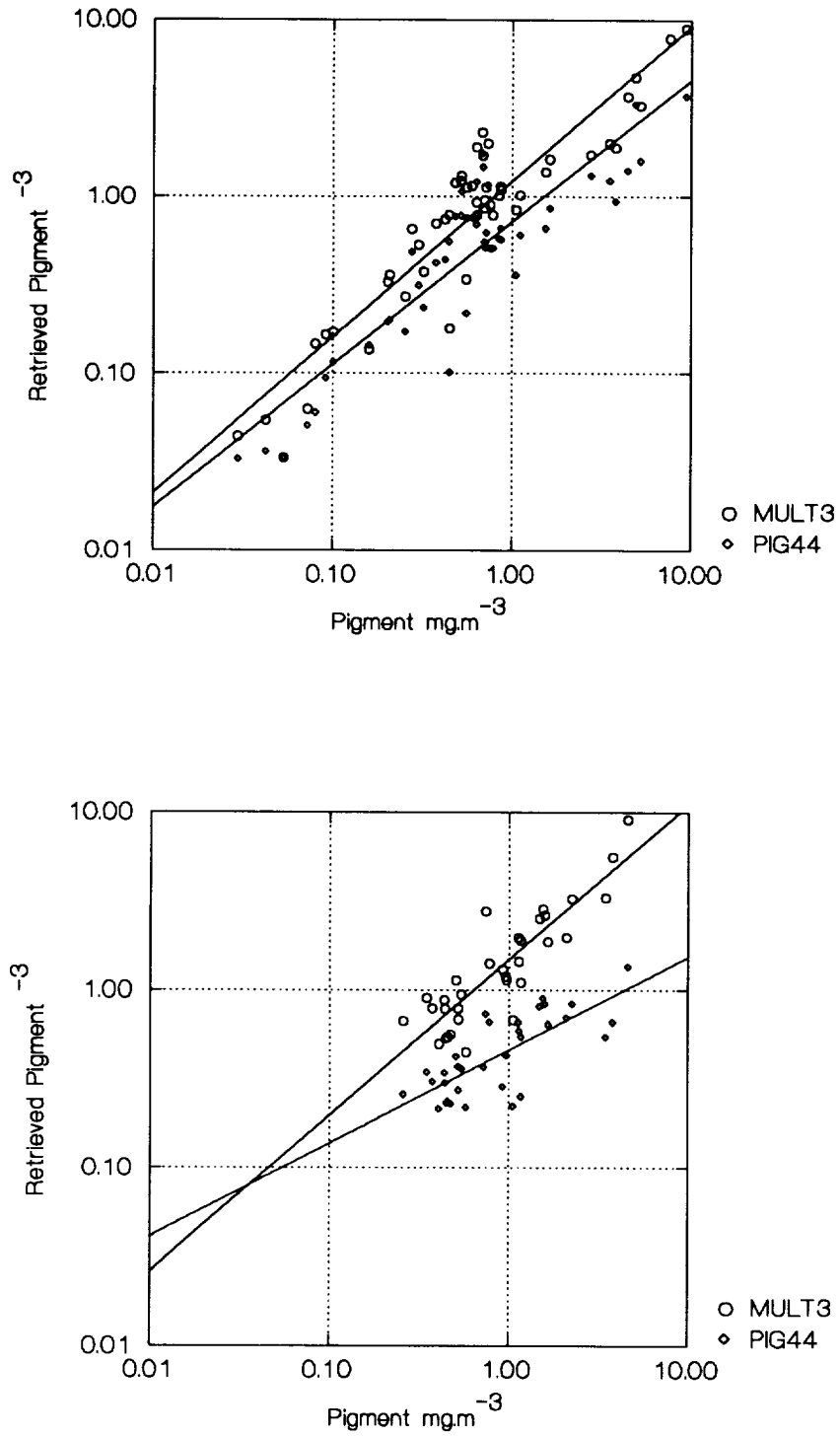
Fig. 11. Hyperbolic multiple regression pigment $[\ln(C_a + C_P) = -0.461H(443{:}555) + 1.821H(490{:}555)$ (circles and upper line) compared with $H(443{:}555)$ derived pigment (diamonds and lower line): **a)** NET data (top) and **b)** Sterna data (bottom).
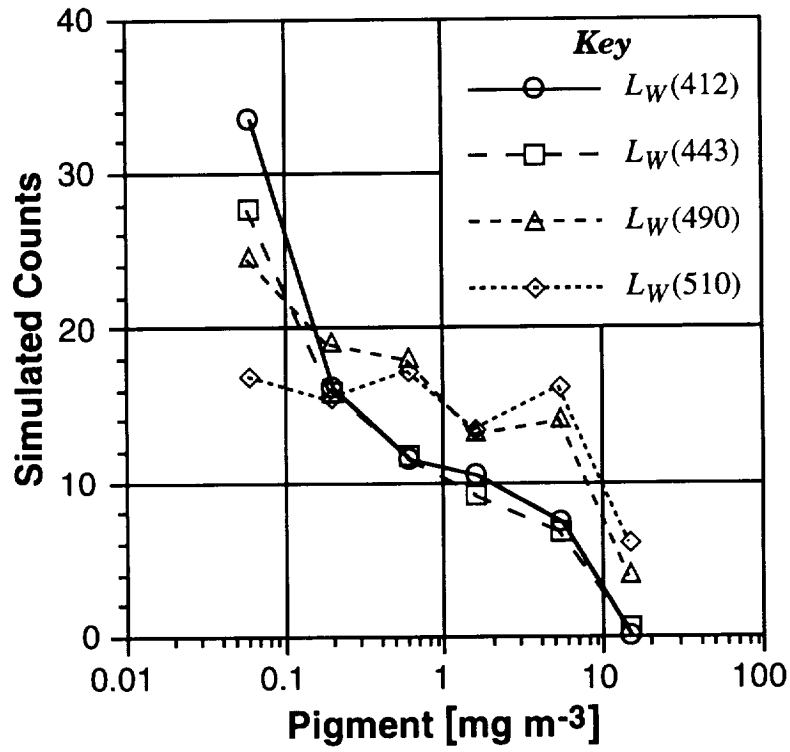
Fig. 12. Mean simulated SeaWiFS counts as a function of pigment, $\log(C_a + C_P)$.
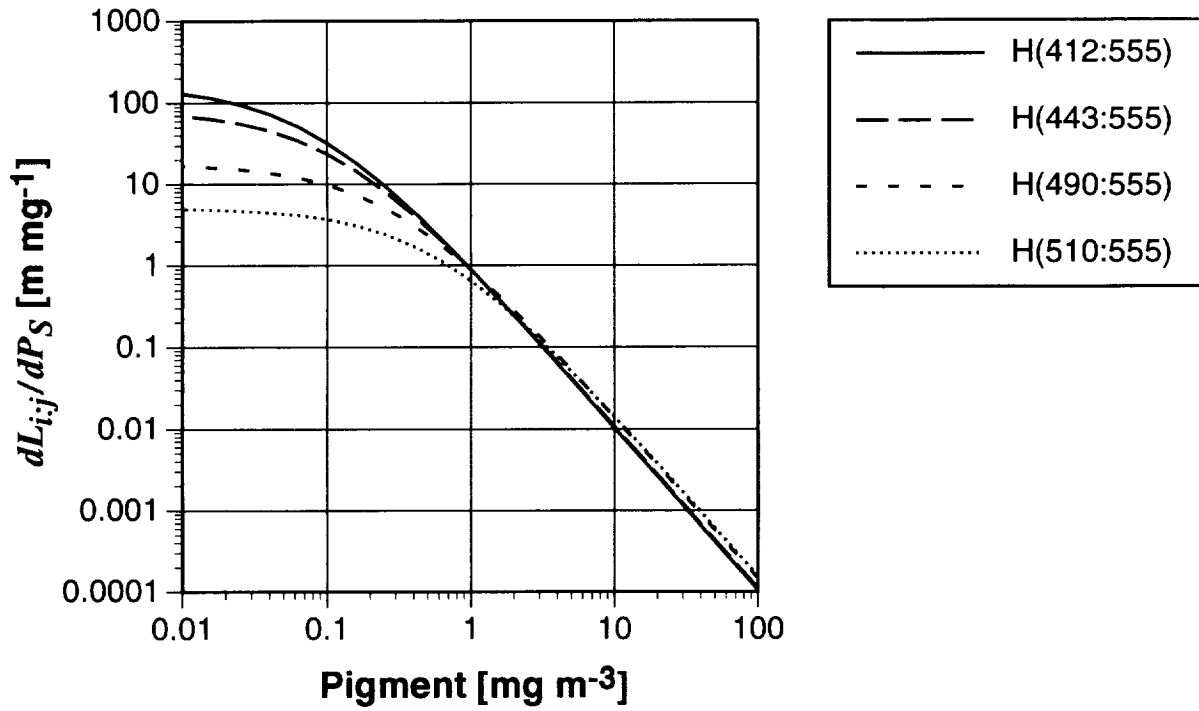
Fig. 13. Derivatives of the hyperbolic model versus P_S.

(POLDER) airborne imagery, to test published models. Morel and Gentili (1993) indicate that for ratios, the effects of viewing off nadir are less severe than for radiance inversion methods; the viewing angle effect is not seen in CZCS images, but some effects may be observed with the greater radiometric precision of SeaWiFS.

The precision of the retrieval can be addressed using both the NET data and the hyperbolic model. The hyperbolic model can be differentiated analytically to show how $dL_{i:j}/dP_S$ varies with pigment. The rate of change in ratio per unit pigment gives the inherent accuracy of the retrievals. Figure 13 shows this rate of change is high for low pigment concentrations, and also shows a log-log decrease with increasing pigment concentration. At low pigment $dL_{i:j}/dP_S$ is higher for the 412:555 and 443:555, but the rate of change is similar for all band ratios at pigments greater the $1\,\text{mg m}^{-3}$. The log-log relationship also indicates that the error structure of the pigment retrievals will be log normal, even if local variability in pigment is normally distributed.

The relative sensitivities shown in Fig. 8 indicate the 412:555 and 443:555 ratios respond to chlorophylls and almost as strongly to DOM, and the 490:555 and 510:555 ratios respond principally to carotenoids, with the 490:555 ratio showing some response to chlorophylls. Figure 14 shows the relationship between total chlorophyll and total carotenoid, showing the ranges of pigment where each band ratio may be used. The carotenoid chlorophyll ratio seems to break down at total chlorophylls below $0.1\,\text{mg m}^{-3}$. This effect may be due to different species assemblages in highly oligotrophic waters (possibly due to phycobiliproteins replacing carotenoids), or it may be an analytical artifact, since the total carotenoids are a sum of a greater number of components, each of which may be below the detection limits of HPLC. More data will be needed to resolve the problem, but the present data suggest some caution is required when using the 490:555 (and 510:555) ratio to determine chlorophyll in oligotrophic waters.

These considerations limit the choice of final algorithm, from those suggested in the previous sections. The following conclusions can be made.

1) If algorithm switching is to be avoided, only combinations of the 490, 510, and 555 bands can be used. Table 17 shows that no multiple regression log algorithm could be derived using these bands. In essence, the 490:555, 490:410, and 510:555 contained no extra information to determine pigment.

2) If algorithm switching can be implemented, then Table 17 indicates the 443:490 and 443:555 ratios can be used. It will not be necessary to use the 412 nm band where atmospheric correction may be a problem.

For the single algorithm, it is a matter of choosing between the 490:555 and 510:555 combinations. Tables 10,

11, and 12 indicated there is no significant difference between the quality of fits of the ratios for either the log or hyperbolic model fit. The pigment relationship shown in Fig. 14 indicates there are biological reasons for considering the 490:555 ratio superior, since its response to chlorophyll will alleviate potential problems in oligotrophic waters. Both the hyperbolic model and log-log fits represent adequate models for the data, but the hyperbolic model shows erroneous retrievals at high chlorophyll where there is little data.

A model constrained with high chlorophyll simulated data has been used to produce a revised set of coefficients for the hyperbolic model. The constrained fits shown in Tables 21 and 22 give a better R^2 for the 490:555 ratio compared with the 510:555 ratio. Using these revised tables, the error structure can be examined. Figure 15 shows the mean residual error for both the hyperbolic model and log-log regression. Although the hyperbolic model performs better at pigments less than $2\,\text{mg m}^{-3}$, the log-log regression covers the whole range of pigment. The final algorithm uses the hyperbolic estimates at low pigment to account for the deviation from log linearity at low chlorophyll (see Fig. 6), and the log-log regression at pigments greater than this.

Table 21. Revised NET data pigment curve fits, where *bands* refer to the band:555 (band 5) ratio.

Band	B	A_1	A_2	R^2
412	13.14	0.019	12.48	88.6
443	9.55	0.045	8.59	89.1
490	5.29	0.112	3.48	87.5
510	3.17	0.140	1.79	84.9

Table 22. Revised NET data chlorophyll curve fits, where *bands* refer to the band:555 (band 5) ratio.

Band	B	A_1	A_2	R^2
412	13.14	0.022	14.45	86.6
443	9.55	0.054	10.31	87.5
490	5.29	0.136	4.23	85.7
510	3.17	0.169	2.16	82.7

This combined method gives an R^2 of 90.9% for pigment compared with R^2 values of 87.5% and 89.6% for the hyperbolic and log regressions, respectively. Although this is only a small improvement over the whole range, for pigment concentrations less than $2\,\text{mg m}^{-3}$ the hyperbolic model gives an R^2 of 82.3% compared with an R^2 of 74.1% for the log regression. This improvement adds considerably to the accuracy of pigment retrievals in oligotrophic waters.

Explicitly, the algorithms for chlorophyll and pigment are computed as follows: 1) The log regressions are determined as

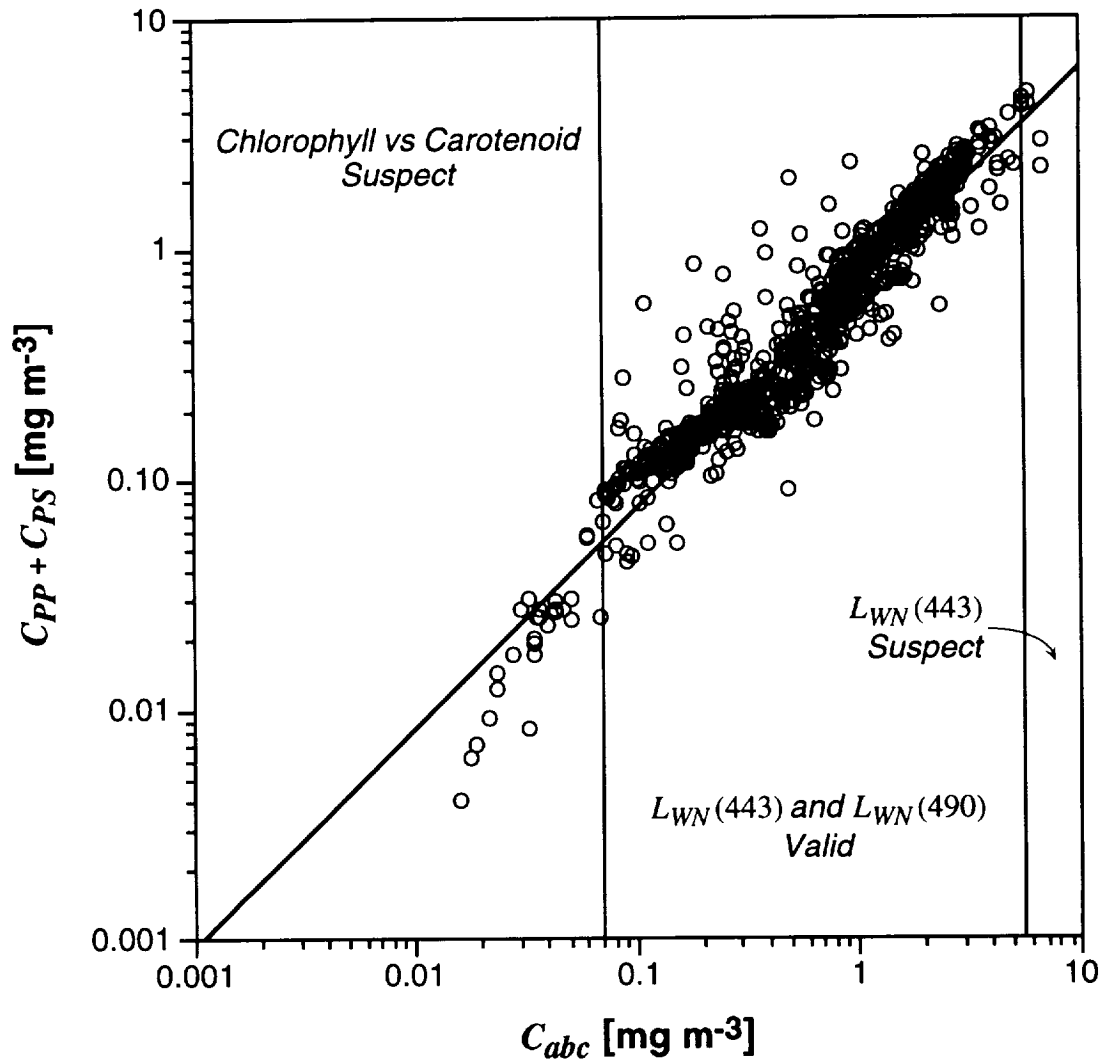$$C_a = \exp\left[0.464 - 1.989\ln\left(\frac{L_{WN}(490)}{L_{WN}(555)}\right)\right] \quad (21)$$

Fig. 14. The global variation of total chlorophyll (C_{abc}) versus carotenoids $(C_{PP} + C_{PS})$, showing the range of validity for $L_{WN}(443)$ and $L_{WN}(490)$; the ranges where the relationship is suspect are to the right and left.
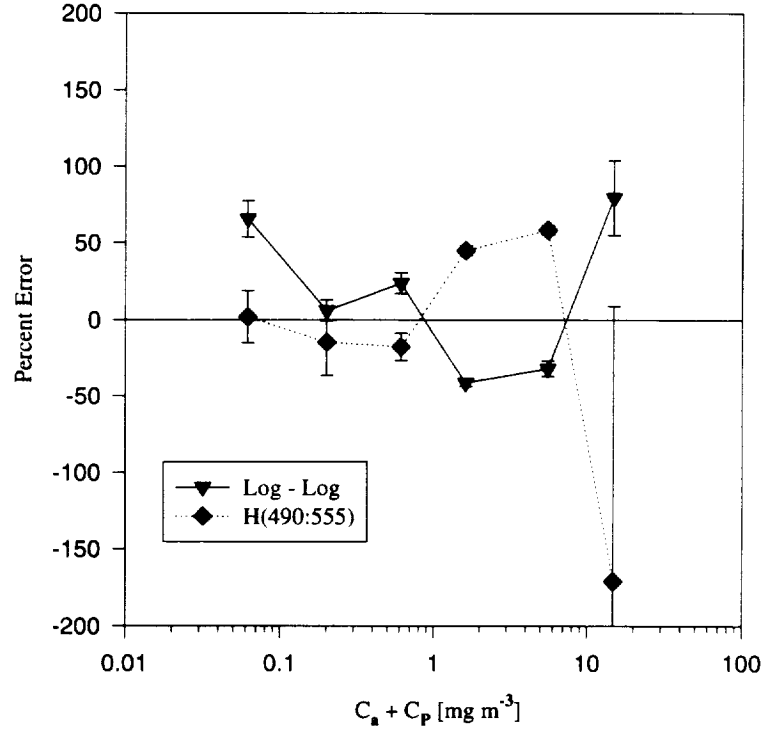
Fig. 15. Percent error in retrieval for the log-log and hyperbolic fits of $C_a + C_P$ for the 490:555 ratio.

and

$$C_a + C_P = \exp\left[0.696 - 2.085\ln\left(\frac{L_{WN}(490)}{L_{WN}(555)}\right)\right]; \quad (22)$$

and 2) if C_a or $C_a + C_P$ are less than $2.0\,\text{mg m}^{-3}$, the inversion of the hyperbolic model, i.e., $C = (L_{i:j} - B)/(A_1B - A_2L_{i:j})$, is used to calculate C_P and C_a as

$$C_a = \frac{\frac{L_{WN}(490)}{L_{WN}(555)} - 5.29}{0.719 - 4.23\frac{L_{WN}(490)}{L_{WN}(555)}} \quad (23)$$

and

$$C_a + C_P = \frac{\frac{L_{WN}(490)}{L_{WN}(555)} - 5.29}{0.592 - 3.48\frac{L_{WN}(490)}{L_{WN}(555)}}. \quad (24)$$

It should be emphasized that the split represents a curve fitting method, rather than a split algorithm. With a more extensive high pigment data set, the hyperbolic model can be better constrained to cover the entire dynamic range of pigment. Figure 16 shows a comparison of the 490:555 ratio algorithm with the OCTS algorithm, the Clark combined ratio model, and the 443:555 ratio algorithm. The algorithm is, as expected, highly sensitive to carotenoids; it shows the least response to Gelbstoff, scattering, and detritus.

Although a number of the multiband algorithms shown in previous sections show high R^2 values, they also display problems when used as inversion algorithms in that they can produce negative retrievals. The final multiband algorithm that was developed avoids these problems; it is based on a correction to the 490:555 ratio algorithm shown above. By using the same band ratios as the hyperbolic multiple pigment algorithms shown in Fig. 11 (see Table 19), this algorithm can be normalized to the pigment retrievals as described below.

The multiple regression algorithm for chlorophyll is:

$$C_a = A_1H(490{:}555) + A_2H(443{:}555) \quad (25)$$

or

$$\frac{C_a}{H(490{:}555)} = A_1 + A_2\left[\frac{H(443{:}555)}{H(490{:}555)}\right], \quad (26)$$

which may be approximated by

$$\frac{C_a}{H(490{:}555)} = A_1'\left[\frac{L_{WN}(443)}{L_{WN}(555)} + A_2'\right]$$

$$= A_1''\left[\frac{L_{WN}(443)}{L_{WN}(555)} + A_2''\right]^{\frac{1}{2}}, \quad (27)$$

where the square root is an arbitrary scaling of the L_{WN} ratio, and A_1 and A_2 are arbitrary constants. The use of the L_{WN} ratio rather than the ratio of the hyperbolic pigments has the advantage of reducing noise, since only two bands are required for the final correction.
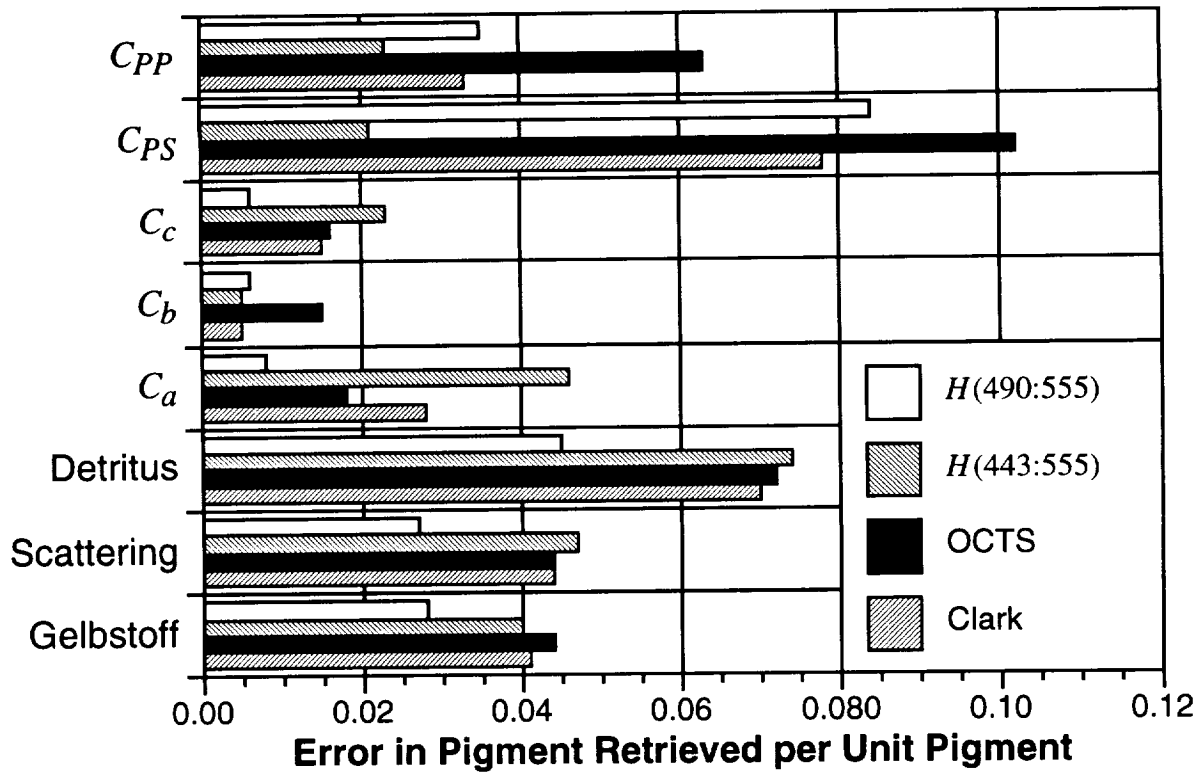
Fig. 16. Relative error in retrieval of $C_a + C_P$ at unit chlorophyll for the recommended 490:555 algorithm, the $H(443:555)$ algorithm, the Ocean Color Temperature Sensor (OCTS) algorithm, and the Clark four-band algorithm at unit pigment for individual biogeochemical measures.

The final algorithm adjustment is

$$C_a' = 1.455 C_a \left[\frac{L_{WN}(443)}{L_{WN}(555)} - 0.279 \right]^{\frac{1}{2}} \quad (28)$$

and

$$C_a' + C_P' = 1.280 [C_a + C_P] \left[\frac{L_{WN}(443)}{L_{WN}(555)} - 0.163 \right]^{\frac{1}{2}} \quad (29)$$

The correction is applied where pigment concentration is less than $2\,\text{mg m}^{-3}$, i.e., when $L_{WN}(443)$ is valid. This corrected pigment concentration results in an overall (0.02–$50\,\text{mg m}^{-3}$) R^2 of 91.1%, and an R^2 of 90.9% when pigment concentration is less than $2\,\text{mg m}^{-3}$. The improvement is 8.6% when compared with the composite single-band algorithm. It is envisaged that when the algorithm is used for biogeochemical provinces with greater variation in pigment type, the algorithm will show a greater improvement in the explained variance.

7. CONCLUSIONS

1. Bio-optical models, show that there is a sound theoretical basis for band-ratio algorithms with explicit solutions which relate to the IOPs of water and its constituents. This indicates that the measurement

of IOPs for algorithm development may be as appropriate as the measument of apparent optical properties (AOPs), e.g., $R(\lambda)$.

2. The BSM developed for this study has proved a powerful tool for the development of algorithms, and has the potential for further parameterization, so as to achieve closure with *in situ* data.

3. Biological coupling, as indexed by the major pigment groups, constrains and restricts the bio-optical variability (i.e., there is less bio-optical variability than would be expected); thus, there are sound grounds for an unbiased composite photosynthetic pigment algorithm.

4. Although globally robust, there is interprovince variability in the chlorophyll to carotenoid ratio. This variability implies that the accuracy of two band single pigment algorithms, e.g., chlorophyll *a* or PSC will be limited. This fact does not affect the utility of global photosynthetic pigment algorithms, however, and provides a basis for constructing high accuracy province-specific algorithms.

5. Factor analysis of band ratio combinations (all Sea-WiFS two-band combinations) demonstrates that discrete band ratios contain the same variance as similar studies using complete spectra.

6. Optimal band ratio combination algorithms provide some measure of confidence that a universal algorithm can be derived (within the bounds of current data sets), i.e., both empirical methods (conclusion 1) and bio-optical models (conclusion 2) point to a similar conclusion with respect to a universal photosynthetic pigment algorithm.

7. Within the radiometric constraints of SeaWiFS, the 490:555 band combination provides the most robust retrieval of pigment or chlorophyll over five decades of pigment level.

8. With the exception of the total pigment regression (Table 19), the BSM data indicates there is no extra information to be gained by using multiband algorithms with CZCS data. The hyperbolic 443:555 and 510:555 (with ammended coefficients) algorithms can be used with CZCS data, as an alternative to log-log regression.

ACKNOWLEDGMENTS

GLOSSARY

AOL Airborne Oceanographic Lidar
AOP Apparent Optical Property

BATS Bermuda Atlantic Time-Series Station
BOAWG Bio-Optical Algorithm Working Group
BOFS Biogeochemical Ocean Flux Study
BSM Bio-Optical Synthetic Model

Case-1 Water whose reflectance is determined solely by absorption.
Case-2 Water whose reflectance is significantly influenced by scattering.
CZCS Coastal Zone Color Scanner

DOM Dissolved Organic Matter

EqPac Equatorial Pacific

GIN Greenland, Iceland, and Norwegian (Seas)

HPLC High Performance Liquid Chromatography

IOP Inherent Optical Property
IR Infrared

NABE North Atlantic Bloom Experiment
NASA National Aeronautics and Space Administration
NEAT Northeast Atlantic
NET NIMBUS Experiment Team
NIMBUS Not an acronym, but a series of NASA experimental weather satellites containing a wide variety of atmosphere, ice, and ocean sensors.

OCTS Ocean Color Temperature Sensor (Japan)

PML Plymouth Marine Laboratory (United Kingdom)
POLDER Polarization and Directionality of the Earth's Reflectances (France)
PPC Photoprotectant Carotenoids
PSC Photosynthetic Carotenoids

SeaWiFS Sea-viewing Wide Field-of-view Sensor
SPO SeaWiFS Project Office
SPSWG SeaWiFS Prelaunch Science Working Group
Sterna Not an acronym, but a BOFS Antarctic research project.

SYMBOLS

$a(\lambda)$ The absorption coefficient.
a' The absorption at the Raman excitation wavelength.
a_a The specific absorption of chlorophyll a.
a_{abc} The specific absorption of chlorophylls a, b, and c.
a_b The specific absorption of chlorophyll b.
a_c The specific absorption of chlorophyll c.
a_g The DOM/detritus specific absorbance.
a_{PP} The specific absorption of PPC.
a_{PS} The specific absorption of PSC.
a_w The absorption coefficient of water.
a_ϕ The DOM/chlorophyll combined absorbance.
A_i An arbitrary constant.
A_j An arbitrary constant.
A_i' An arbitrary constant.
A_j' An arbitrary constant.

$b_b(\lambda)$ The backscatter coefficient.
b_{bp} The particle specific backscatter coefficient (usually normalized to chlorophyll a concentration).
b_{bw} The backscatter coefficient of water.
b_{min} Scattering associated with phytoplankton (Prieur and Sathyendranath, 1981).
b_R The Raman scattering coefficient.
B An empirical constant.
B_b An empirical constant dependant on the backscatter ratio.

$c(\lambda)$ The spectral attenuation coefficient.
C Chlorophyll concentration.
C_a The concentration of chlorophyll a.
C_{abc} The concentration of chlorophylls a, b, and c.
C_b The concentration of chlorophyll b.
C_c The concentration of chlorophyll c.
C_P Phaeopigment concentration.
C_{PP} PPC concentration.
C_{PS} PSC concentration.
C_S Simulated C.
C_{TP} Total pigment concentration.

E_0' The downwelling irradiance at the Raman excitation wavelength.

F_0 Extra terrestrial irradiance.
F_1 Pigment biomass loading factor.
F_2 Detritus concentration loading factor.
F_3 Carotenoid concentration (or relative pigment abundance) loading factor.

g A constant that consists of the ratios of the air-sea interface effects, the effects of the light field, and the relative spectral variation of Q.
G The concentration of DOM and DOM-like absorbers.
$G(\mu_0, \lambda)$ The effect of the downwelling light field.

$H(\lambda_i{:}\lambda_j)$ Pigment calculated from the hyperbolic transform of $L_{i:j}$.

k An index to two vectors of band ratios k_1 and k_2.
k_1 A band ratio vector.
k_2 A band ratio vector.

$L_{i:j}$ The ratio of normalized water-leaving radiances at wavelengths i (λ_i) to j (λ_j): $L_{WN}(\lambda_i)/L_{WN}(\lambda_j)$.
$L_{WN}(\lambda)$ Normalized water-leaving radiance.
L'_{WN} Normalized water-leaving radiance at the Raman excitation wavelength.

n The index of refraction.

P The particulate concentration including detrital material.
P_S Simulated $C_a + C_P$ (q.v.).

Q The ratio of upwelling irradiance to radiance, which varies with the angular distribution of the upwelling light field, and is π for an isotropic distribution.

r The air-water reflectance for diffuse irradiance.
R^2 The regression coefficient.
$R(\lambda)$ The irradiance reflectance at a particular wavelength.

S The slope of a line.

α' A power law constant.
α_0 A curve fitting constant.
α_1 A curve fitting constant.
α_2 A curve fitting constant.

β' A power law constant.

λ' Raman excitation wavelength.
λ_i Wavelength of light at a particular band.
λ_j Wavelength of light at a particular band.

ρ The Fresnel reflectance at normal incidence.
$\tilde{\rho}$ The Fresnel reflectance for sun and sky irradiance.

REFERENCES

Aiken, J., and G. Moore, 1995: Special requirements for the validation of ocean colour information. Proceedings of the WMO/IOC Conference on Space-Based Ocean Observation, WMO/PD-No. 649, 93–101.

——, G. Moore, and P. Holligan, 1992: Remote sensing of oceanographic biology in relation to global climate change. J. Phycol., 28, 579–590.

Barnes, R.A., A.W. Holmes, W.L. Barnes, W.E. Esaias, C.R. McClain, and T. Svitek, 1994: SeaWiFS Prelaunch Radiometric Calibration and Spectral Characterization. NASA Tech. Memo. 104566, Vol. 23, S.B. Hooker, E.R. Firestone, and J.G. Acker, Eds., NASA Goddard Space Flight Center, Greenbelt, Maryland, 55 pp.

Bidigare, R.R., M.E. Ondrusek, J.H. Morrow, and D.A. Kiefer, 1990: In vivo absorption properties of algal pigments. SPIE Ocean Optics, 1302, 290–302.

Bricaud, A., A. Morel, and L. Prieur, 1981: Absorption by dissolved organic matter of the sea (yellow substance) in the UV and visible domains. Limnol. Oceanol., 26, 45–53.

Carder, K.L., R.G. Steward, J.H. Paul, and G.A. Vargo, 1986: Relationships between chlorophyll and ocean color constituents as they affect remote-sensing reflectance models. Limnol. Oceanogr., 31, 403–413.

——, R.G. Steward, G.R. Harvey, and P.B. Ortner, 1989: Marine humic and fulvic acids: Their effects on remote sensing of ocean chlorophyll. Limnol. Oceanogr., 34, 38–81.

Clark, D.K., 1981: Phytoplankton pigment algorithms for the Nimbus-7 CZCS. Oceanography from Space, J.F.R. Gower, Ed., Plenum Press, 227–238.

Duysens, L.N.M., 1956: The flattening of the absorption spectrum of suspensions as compared with that of solutions. Biochim. Biophys. Acta., 19, 255, 257, 261.

Garver, S.A., D.A. Siegel, and B.G. Mitchell, 1995: Variability in near surface particulate absorption spectra: What can a satellite imager see? Limnol. Oceanogr., 39, 1,349–1,367.

Gordon, H.R., O.B. Brown, R.H. Evans, J.W. Brown, R.C. Smith, K.S. Baker, and D.K. Clark, 1988: A semianalytic radiance model of ocean color. J. of Geophys. Res., 93, 10,909–10,924.

Hoepffner, N., and S. Sathendranath, 1992: Bio-optical characteristics of coastal waters: Absorption spectra of phytoplankton and pigment distribution in the Western North Atlantic. Limnol. Oceanogr., 37, 1,660–1,679.

Hoepffner, N., and S. Sathyendranath, 1993: Determination of the major groups of phytoplankton pigments from the absorption spectra of total particulate matter. J. Geophys. Res., 98, 22,789–22,803.

Hoge, F.E., and R.E. Swift, 1993: The influence of chlorophyll pigment upon the upwelling spectral radiances from the North Atlantic Ocean. Deep-Sea Res., 40, 265–278.

Holligan, P.M., E. Fernandez, J. Aiken, W.B. Balch, P. Boyd, P.H. Burkill, M. Finch, S.B. Groom, G. Malin, K. Muller, D.A. Purdie, and C. Robinson, 1993: A biogeochemical study of Emiliania huxleyi, in the North Atlantic. Global Biogeochemical Cycles, 7, 879–900.

Hooker, S.B., C.R. McClain, and A. Holmes, 1993: Ocean color imaging: CZCS to SeaWiFS. Marine. Tech. Soc. J., 27, 3–15.

Mantoura, R.F.C., and C.A. Llewellyn, 1983: The rapid determination of algal chlorophyll and carotenoid pigments and their breakdown products in natural waters by reversephase high-performance liquid chromatography. Anal. Chim. Acta., 151, 297–314.

Marshall, B.R., and R.C. Smith, 1990: Raman scattering and in-water ocean optical properties. Appl. Opt., 29, 71–84.

Mitchell, B.G., and O. Holm-Hansen, 1991: Bio-optical properties of Antarctic Peninsula waters: differentiation from temperate ocean models. *Deep-Sea Res.*, **39**, 1,009–1,028.

Morel, A., 1974: Optical properties of pure water and sea water. *Optical Aspects of Oceanography*, N.G. Jerlov and S. Nielsen, Eds., Academic Press, 1–24.

——, and L. Prieur, 1977: Analysis of variation in ocean colour. *Limnol. Oceanogr.*, **22**, 709–722.

——, and B. Gentili, 1991: Diffuse reflectance of oceanic waters. I. Its dependence on sun angle as influenced by the molecular scattering contribution. *Appl. Opt.*, **30**, 4,427–4,438.

——, and B. Gentili, 1993: Diffuse reflectance of oceanic waters. II. Bidirectional aspects. *Appl. Opt.*, **32**, 6,864–6,879.

Mueller, J.L., 1976: Ocean color spectra measured off the Oregon coast: characteristic vectors. *Appl. Opt.*, **15**, 394–402.

——, and R.W. Austin, 1995: Ocean Optics Protocols for SeaWiFS Validation, Revision 1. *NASA Tech. Memo. 104566, Vol. 25*, S.B. Hooker, E.R. Firestone, and J.G. Acker, Eds., NASA Goddard Space Flight Center, Greenbelt, Maryland, 66 pp.

Petzold, T.J., 1972: Volume scattering functions for selected ocean waters. *Scripps Inst. Oceanogr. Rep. 72–78*, 79 pp.

Prieur, L., and S. Sathyendranath, 1981: An optical classification of coastal and oceanic waters based on the specific spectral absorption curves of phytoplankton pigments, dissolved organic matter, and other particulate materials. *Limnol. Oceanogr.*, **26**, 671–689.

Sathyendranath, S., 1981: *Influence des substances en solution et en suspension dans les eaux de mer sur l'absorption et la reflectance. Modelisation et application a la teledetection.* Ph.D. Thesis, University of Paris, 123 pp (in French).

Smith, R.C., and K.S. Baker, 1981: Optical properties of the clearest natural waters (200–800 nm). *Appl. Opt.*, **20**, 177–184.

Strickland, J.D.H., and T.R. Parsons, 1972: *A Practical Handbook of Sea Water Analysis*. Fish. Res. Board. Canada, 310 pp.

Sullivan, C.W., K.R. Arrigo, C.R. McClain, J.C. Comiso, and J.K. Firestone, 1993: Distributions of phytoplankton blooms in the Southern Ocean. *Science*, **262**, 1,832–1,837.

Trees, C.C., M.C. Kenicutt, and J.M. Brooks, 1985: Errors associated with the standard fluorometric determination of chlorophylls and phaeopigments. *Mar. Chem.*, **17**, 1–12.

——, D.K. Clark, R. Bidigare, and M. Ondrusek, 1995: Chlorophyll *a* versus accessory pigment concentrations within the euphotic zone: A ubiquitous relationship? *Science*, (submitted).

Yentsch, C.S., and D.W. Menzel, 1963: A method for determination of phytoplankton, chlorophyll and phaeophytin by fluorescence. *Deep-Sea Res.*, **10**, 221–231.

THE SeaWiFS TECHNICAL REPORT SERIES

<u>*Vol. 1*</u>

Hooker, S.B., W.E. Esaias, G.C. Feldman, W.W. Gregg, and C.R. McClain, 1992: An Overview of SeaWiFS and Ocean Color. *NASA Tech. Memo. 104566, Vol. 1*, S.B. Hooker and E.R. Firestone, Eds., NASA Goddard Space Flight Center, Greenbelt, Maryland, 24 pp., plus color plates.

<u>*Vol. 2*</u>

Gregg, W.W., 1992: Analysis of Orbit Selection for SeaWiFS: Ascending vs. Descending Node. *NASA Tech. Memo. 104566, Vol. 2*, S.B. Hooker and E.R. Firestone, Eds., NASA Goddard Space Flight Center, Greenbelt, Maryland, 16 pp.

<u>*Vol. 3*</u>

McClain, C.R., W.E. Esaias, W. Barnes, B. Guenther, D. Endres, S. Hooker, G. Mitchell, and R. Barnes, 1992: Calibration and Validation Plan for SeaWiFS. *NASA Tech. Memo. 104566, Vol. 3*, S.B. Hooker and E.R. Firestone, Eds., NASA Goddard Space Flight Center, Greenbelt, Maryland, 41 pp.

<u>*Vol. 4*</u>

McClain, C.R., E. Yeh, and G. Fu, 1992: An Analysis of GAC Sampling Algorithms: A Case Study. *NASA Tech. Memo. 104566, Vol. 4*, S.B. Hooker and E.R. Firestone, Eds., NASA Goddard Space Flight Center, Greenbelt, Maryland, 22 pp., plus color plates.

<u>*Vol. 5*</u>

Mueller, J.L., and R.W. Austin, 1992: Ocean Optics Protocols for SeaWiFS Validation. *NASA Tech. Memo. 104566, Vol. 5*, S.B. Hooker and E.R. Firestone, Eds., NASA Goddard Space Flight Center, Greenbelt, Maryland, 43 pp.

<u>*Vol. 6*</u>

Firestone, E.R., and S.B. Hooker, 1992: SeaWiFS Technical Report Series Summary Index: Volumes 1–5. *NASA Tech. Memo. 104566, Vol. 6*, S.B. Hooker and E.R. Firestone, Eds., NASA Goddard Space Flight Center, Greenbelt, Maryland, 9 pp.

<u>*Vol. 7*</u>

Darzi, M., 1992: Cloud Screening for Polar Orbiting Visible and IR Satellite Sensors. *NASA Tech. Memo. 104566, Vol. 7*, S.B. Hooker and E.R. Firestone, Eds., NASA Goddard Space Flight Center, Greenbelt, Maryland, 7 pp.

<u>*Vol. 8*</u>

Hooker, S.B., W.E. Esaias, and L.A. Rexrode, 1993: Proceedings of the First SeaWiFS Science Team Meeting. *NASA Tech. Memo. 104566, Vol. 8*, S.B. Hooker and E.R. Firestone, Eds., NASA Goddard Space Flight Center, Greenbelt, Maryland, 61 pp.

<u>*Vol. 9*</u>

Gregg, W.W., F.C. Chen, A.L. Mezaache, J.D. Chen, J.A. Whiting, 1993: The Simulated SeaWiFS Data Set, Version 1. *NASA Tech. Memo. 104566, Vol. 9*, S.B. Hooker, E.R. Firestone, and A.W. Indest, Eds., NASA Goddard Space Flight Center, Greenbelt, Maryland, 17 pp.

Vol. 10

Woodward, R.H., R.A. Barnes, C.R. McClain, W.E. Esaias, W.L. Barnes, and A.T. Mecherikunnel, 1993: Modeling of the SeaWiFS Solar and Lunar Observations. *NASA Tech. Memo. 104566, Vol. 10,* S.B. Hooker and E.R. Firestone, Eds., NASA Goddard Space Flight Center, Greenbelt, Maryland, 26 pp.

Vol. 11

Patt, F.S., C.M. Hoisington, W.W. Gregg, and P.L. Coronado, 1993: Analysis of Selected Orbit Propagation Models for the SeaWiFS Mission. *NASA Tech. Memo. 104566, Vol. 11,* S.B. Hooker, E.R. Firestone, and A.W. Indest, Eds., NASA Goddard Space Flight Center, Greenbelt, Maryland, 16 pp.

Vol. 12

Firestone, E.R., and S.B. Hooker, 1993: SeaWiFS Technical Report Series Summary Index: Volumes 1–11. *NASA Tech. Memo. 104566, Vol. 12,* S.B. Hooker and E.R. Firestone, Eds., NASA Goddard Space Flight Center, Greenbelt, Maryland, 28 pp.

Vol. 13

McClain, C.R., K.R. Arrigo, J. Comiso, R. Fraser, M. Darzi, J.K. Firestone, B. Schieber, E-n. Yeh, and C.W. Sullivan, 1994: Case Studies for SeaWiFS Calibration and Validation, Part 1. *NASA Tech. Memo. 104566, Vol. 13,* S.B. Hooker and E.R. Firestone, Eds., NASA Goddard Space Flight Center, Greenbelt, Maryland, 52 pp., plus color plates.

Vol. 14

Mueller, J.L., 1993: The First SeaWiFS Intercalibration Round-Robin Experiment, SIRREX-1, July 1992. *NASA Tech. Memo. 104566, Vol. 14,* S.B. Hooker and E.R. Firestone, Eds., NASA Goddard Space Flight Center, Greenbelt, Maryland, 60 pp.

Vol. 15

Gregg, W.W., F.S. Patt, and R.H. Woodward, 1994: The Simulated SeaWiFS Data Set, Version 2. *NASA Tech. Memo. 104566, Vol. 15,* S.B. Hooker and E.R. Firestone, Eds., NASA Goddard Space Flight Center, Greenbelt, Maryland, 42 pp., plus color plates.

Vol. 16

Mueller, J.L., B.C. Johnson, C.L. Cromer, J.W. Cooper, J.T. McLean, S.B. Hooker, and T.L. Westphal, 1994: The Second SeaWiFS Intercalibration Round-Robin Experiment, SIRREX-2, June 1993. *NASA Tech. Memo. 104566, Vol. 16,* S.B. Hooker and E.R. Firestone, Eds., NASA Goddard Space Flight Center, Greenbelt, Maryland, 121 pp.

Vol. 17

Abbott, M.R., O.B. Brown, H.R. Gordon, K.L. Carder, R.E. Evans, F.E. Muller-Karger, and W.E. Esaias, 1994: Ocean Color in the 21st Century: A Strategy for a 20-Year Time Series. *NASA Tech. Memo. 104566, Vol. 17,* S.B. Hooker and E.R. Firestone, Eds., NASA Goddard Space Flight Center, Greenbelt, Maryland, 20 pp.

Vol. 18

Firestone, E.R., and S.B. Hooker, 1995: SeaWiFS Technical Report Series Summary Index: Volumes 1–17. *NASA Tech. Memo. 104566, Vol. 18,* S.B. Hooker and E.R. Firestone, Eds., NASA Goddard Space Flight Center, Greenbelt, Maryland, 47 pp.

Vol. 19

McClain, C.R., R.S. Fraser, J.T. McLean, M. Darzi, J.K. Firestone, F.S. Patt, B.D. Schieber, R.H. Woodward, E-n. Yeh, S. Mattoo, S.F. Biggar, P.N. Slater, K.J. Thome, A.W. Holmes, R.A. Barnes, and K.J. Voss, 1994: Case Studies for SeaWiFS Calibration and Validation, Part 2. *NASA Tech. Memo. 104566, Vol. 19,* S.B. Hooker, E.R. Firestone, and J.G. Acker, Eds., NASA Goddard Space Flight Center, Greenbelt, Maryland, 73 pp.

Vol. 20

Hooker, S.B., C.R. McClain, J.K. Firestone, T.L. Westphal, E-n. Yeh, and Y. Ge, 1994: The SeaWiFS Bio-Optical Archive and Storage System (SeaBASS), Part 1. *NASA Tech. Memo. 104566, Vol. 20,* S.B. Hooker and E.R. Firestone, Eds., NASA Goddard Space Flight Center, Greenbelt, Maryland, 40 pp.

Vol. 21

Acker, J.G., 1994: The Heritage of SeaWiFS: A Retrospective on the CZCS NIMBUS Experiment Team (NET) Program. *NASA Tech. Memo. 104566, Vol. 21,* S.B. Hooker and E.R. Firestone, Eds., NASA Goddard Space Flight Center, Greenbelt, Maryland, 43 pp.

Vol. 22

Barnes, R.A., W.L. Barnes, W.E. Esaias, and C.R. McClain, 1994: Prelaunch Acceptance Report for the SeaWiFS Radiometer. *NASA Tech. Memo. 104566, Vol. 22,* S.B. Hooker, E.R. Firestone, and J.G. Acker, Eds., NASA Goddard Space Flight Center, Greenbelt, Maryland, 32 pp.

Vol. 23

Barnes, R.A., A.W. Holmes, W.L. Barnes, W.E. Esaias, C.R. McClain, and T. Svitek, 1994: SeaWiFS Prelaunch Radiometric Calibration and Spectral Characterization. *NASA Tech. Memo. 104566, Vol. 23,* S.B. Hooker, E.R. Firestone, and J.G. Acker, Eds., NASA Goddard Space Flight Center, Greenbelt, Maryland, 55 pp.

Vol. 24

Firestone, E.R., and S.B. Hooker, 1995: SeaWiFS Technical Report Series Summary Index: Volumes 1–23. *NASA Tech. Memo. 104566, Vol. 24,* S.B. Hooker and E.R. Firestone, Eds., NASA Goddard Space Flight Center, Greenbelt, Maryland, 36 pp.

Vol. 25

Mueller, J.L., and R.W. Austin, 1995: Ocean Optics Protocols for SeaWiFS Validation, Revision 1. *NASA Tech. Memo. 104566, Vol. 25,* S.B. Hooker and E.R. Firestone, Eds., NASA Goddard Space Flight Center, Greenbelt, Maryland, 66 pp.

Vol. 26

Siegel, D.A., M.C. O'Brien, J.C. Sorensen, D.A. Konnoff, E.A. Brody, J.L. Mueller, C.O. Davis, W.J. Rhea, and S.B. Hooker, 1995: Results of the SeaWiFS Data Analysis Round-Robin (DARR), July 1994. *NASA Tech. Memo. 104566, Vol. 26,* S.B. Hooker and E.R. Firestone, Eds., NASA Goddard Space Flight Center, Greenbelt, Maryland, 58 pp.

Vol. 27

J.L. Mueller, R.S. Fraser, S.F. Biggar, K.J. Thome, P.N. Slater, A.W. Holmes, R.A. Barnes, C.T. Weir, D.A. Siegel, D.W. Menzies, A.F. Michaels, and G. Podesta, 1995: Case Studies for SeaWiFS Calibration and Validation, Part 3. *NASA Tech. Memo. 104566, Vol. 27,* S.B. Hooker, E.R. Firestone, and J.G. Acker, Eds., NASA Goddard Space Flight Center, Greenbelt, Maryland, 46 pp.

Vol. 28

McClain, C.R., K.R. Arrigo, W.E. Esaias, M. Darzi, F.S. Patt, R.H. Evans, J.W. Brown, C.W. Brown, R.A. Barnes, and L. Kumar, 1995: SeaWiFS Algorithms, Part 1. *NASA Tech. Memo. 104566, Vol. 28,* S.B. Hooker, E.R. Firestone, and J.G. Acker, Eds., NASA Goddard Space Flight Center, Greenbelt, Maryland, 38 pp., plus color plates.

Vol. 29

Aiken, J., G.F. Moore, C.C. Trees, S.B. Hooker, and D.K. Clark, 1995: The SeaWiFS CZCS-Type Pigment Algorithm. *NASA Tech. Memo. 104566, Vol. 29,* S.B. Hooker and E.R. Firestone, Eds., NASA Goddard Space Flight Center, Greenbelt, Maryland, 34 pp.

REPORT DOCUMENTATION PAGE

Form Approved
OMB No. 0704-0188

Public reporting burden for this collection of information is estimated to average 1 hour per response, including the time for reviewing instructions, searching existing data sources, gathering and maintaining the data needed, and completing and reviewing the collection of information. Send comments regarding this burden estimate or any other aspect of this collection of information, including suggestions for reducing this burden, to Washington Headquarters Services, Directorate for Information Operations and Reports, 1215 Jefferson Davis Highway, Suite 1204, Arlington, VA 22202-4302, and to the Office of Management and Budget, Paperwork Reduction Project (0704-0188), Washington, DC 20503.

1. AGENCY USE ONLY *(Leave blank)*	2. REPORT DATE June 1995	3. REPORT TYPE AND DATES COVERED Technical Memorandum

4. TITLE AND SUBTITLE
SeaWiFS Technical Report Series
Volume 29–The SeaWiFS CZCS-Type Pigment Algorithm

5. FUNDING NUMBERS
Code 970.2

6. AUTHOR(S)
James Aiken, Gerald F. Moore, Charles C. Trees, Stanford B. Hooker, and Dennis K. Clark
Series Editors: Stanford B. Hooker and Elaine R. Firestone

7. PERFORMING ORGANIZATION NAME(S) AND ADDRESS(ES)

Laboratory for Hydrospheric Processes
Goddard Space Flight Center
Greenbelt, Maryland 20771

8. PERFORMING ORGANIZATION REPORT NUMBER

95B00096

9. SPONSORING/MONITORING AGENCY NAME(S) AND ADDRESS(ES)

National Aeronautics and Space Administration
Washington, D.C. 20546–0001

10. SPONSORING/MONITORING AGENCY REPORT NUMBER

TM–104566, Vol. 29

11. SUPPLEMENTARY NOTES Elaine R. Firestone: General Sciences Corporation, Laurel, Maryland; James Aiken and Gerald Moore: Plymouth Marine Laboratory, Plymouth, United Kingdom; Charles C. Trees: San Diego State University, San Diego, California; Dennis K. Clark: NOAA/National Environmental Satellite Data Information Service, Camp Springs, Maryland

12a. DISTRIBUTION/AVAILABILITY STATEMENT
Unclassified–Unlimited
Subject Category 48
Report is available from the Center for AeroSpace Information (CASI),
800 Elkridge Landing Road, Linthicum Heights, MD 21090; (301)621-0390

12b. DISTRIBUTION CODE

13. ABSTRACT *(Maximum 200 words)*

The Sea-viewing Wide Field-of-view Sensor (SeaWiFS) mission will provide operational ocean color that will be superior to the previous Coastal Zone Color Sensor (CZCS) proof-of-concept mission. An algorithm is needed that exploits the full functionality of SeaWiFS whilst remaining compatible in concept with algorithms used for the CZCS. This document describes the theoretical rationale of radiance band-ratio methods for determining chlorophyll a and other important biogeochemical parameters, and their implementation for the SeaWIFS mission. Pigment interrelationships are examined to explain the success of the CZCS algorithms. In the context where chlorophyll a absorbs only weakly at 520 nm, the success of the 520 nm to 550 nm CZCS band ratio needs to be explained. This is explained by showing that in pigment data from a range of oceanic provinces chlorophyll a (absorbing at less than 490 nm), carotenoids (absorbing at greater than 460 nm), and total pigment are highly correlated. Correlations within pigment groups particularly photoprotectant and photosynthetic carotenoids are less robust. The sources of variability in optical data are examined using the NIMBUS Experiment Team (NET) bio-optical data set and bio-optical model. In both the model and NET data, the majority of the variance in the optical data is attributed to variability in pigment (chlorophyll a, and total particulates, with less than 5% of the variability resulting from pigment assemblage. The relationships between band ratios and chlorophyll is examined analytically, and a new formulation based on a dual hyperbolic model is suggested which gives a better calibration curve than the conventional log-log linear regression fit. The new calibration curve shows the 490:555 ratio is the best single-band ratio and is the recommended CZCS-type pigment algorithm. Using both the model and NET data, a number of multiband algorithms are developed; the best of which is an algorithm based on the 443:555 and 490:555 ratios. From model data, the form of potential algorithms for other products, such as total particulates and dissolved organic matter (DOM), are suggested.

14. SUBJECT TERMS
SeaWiFS, Oceanography, Algorithms, Pigments, CZCS, Band-Ratio, Bio-Optical Models
Data Analyses, NET Data

15. NUMBER OF PAGES
34

16. PRICE CODE

17. SECURITY CLASSIFICATION OF REPORT	18. SECURITY CLASSIFICATION OF THIS PAGE	19. SECURITY CLASSIFICATION OF ABSTRACT	20. LIMITATION OF ABSTRACT
Unclassified	Unclassified	Unclassified	Unlimited

NSN 7540-01-280-5500

Standard Form 298 (Rev. 2-89)